JCB Journal of Cell Biology

ARTICLE

A polybasic domain in aPKC mediates Par6-dependent control of membrane targeting and kinase activity

Wei Dong[1], Juan Lu[1], Xuejing Zhang[1], Yan Wu[2], Kaela Lettieri[3], Gerald R. Hammond[1], and Yang Hong[1]

Mechanisms coupling the atypical PKC (aPKC) kinase activity to its subcellular localization are essential for cell polarization. Unlike other members of the PKC family, aPKC has no well-defined plasma membrane (PM) or calcium binding domains, leading to the assumption that its subcellular localization relies exclusively on protein–protein interactions. Here we show that in both *Drosophila* and mammalian cells, the pseudosubstrate region (PSr) of aPKC acts as a polybasic domain capable of targeting aPKC to the PM via electrostatic binding to PM PI4P and PI(4,5)P_2. However, physical interaction between aPKC and Par-6 is required for the PM-targeting of aPKC, likely by allosterically exposing the PSr to bind PM. Binding of Par-6 also inhibits aPKC kinase activity, and such inhibition can be relieved through Par-6 interaction with apical polarity protein Crumbs. Our data suggest a potential mechanism in which allosteric regulation of polybasic PSr by Par-6 couples the control of both aPKC subcellular localization and spatial activation of its kinase activity.

Introduction

Polarity proteins play conserved and essential roles in regulation of cell polarity, and for the majority of them, achieving polarized plasma membrane (PM)/cortical localization is essential for their functions (Hong, 2018; Rodriguez-Boulan and Macara, 2014). Mechanisms mediating the PM/cortical association of these polarity proteins had often been assumed to be based primarily on the intricate protein–protein interactions among polarity proteins and their regulators (Rodriguez-Boulan and Macara, 2014). Recent studies, however, discovered that several polarity proteins such as Lethal giant larvae (Lgl), Numb, and Miranda contain so-called polybasic (i.e., basic-hydrophobic) domains (Bailey and Prehoda, 2015; Dong et al., 2015), which are short but highly positively charged owing to their enrichment of basic Arg/Lys residues. Polybasic domains can specifically bind to PM, as the inner surface of PM is the most negatively charged membrane surface, as a result of membrane phosphatidylserine (Yeung et al., 2008) and the unique enrichment of polyphosphoinositides phosphatidylinositol-4-phosphate (PI4P) and phosphatidylinositol 4,5-bisphosphate (PIP_2; Hammond et al., 2012). Moreover, polybasic domains in Lgl, Numb, and Miranda also contain conserved serine residues that can be phosphorylated by another key polarity protein, atypical PKC (aPKC; Bailey and Prehoda, 2015; Dong et al., 2015). Similar to the phosphorylation of the polybasic ED domain in myristoylated alanine rich C-kinase substrate (MARCKS) by PKC (Arbuzova et al., 2002), aPKC phosphorylation neutralizes the positive charges in a polybasic domain, therefore inhibiting its electrostatic binding to the PM (Bailey and Prehoda, 2015; Dong et al., 2015). Such aPKC-dependent inhibition serves as an elegant mechanism to polarize the PM targeting of polybasic polarity proteins, allowing apically localized aPKC to limit Lgl, Numb, and Miranda to basolateral PM. Potential aPKC-phosphorylatable polybasic domains have been found in hundreds of proteins in metazoan genomes (Bailey and Prehoda, 2015; Y. Hong, unpublished data), suggesting that aPKC plays a critical role in regulating the PM targeting of many polybasic proteins.

To date, however, the exact molecular mechanism governing the PM/cortical localization of aPKC itself remains unclear. Unlike conventional PKC (cPKC) and novel PKC (nPKC) that bind DAG, phospholipids, and calcium for their kinase activation and PM targeting, aPKC has no well-defined PM or calcium binding domains and has not been demonstrated or proposed to directly bind the PM (Rosse et al., 2010; Garg et al., 2014). In fact, it is considered a unique feature of aPKC that its kinase activity and subcellular localizations appear to be exclusively regulated

[1]Department of Cell Biology, University of Pittsburgh Medical School, Pittsburgh, PA; [2]Jiangsu University, Zhengjiang, Jiangsu, People's Republic of China; [3]First Experience in Research Program, University of Pittsburgh, Pittsburgh, PA.

Correspondence to Yang Hong: yhong@pitt.edu; Kaela Lettieri: ksl47@pitt.edu.

by protein–protein interactions other than lipids and/or calcium (Rosse et al., 2010). aPKC has a PB1 domain that binds to the PB1 domain in another polarity protein, partitioning defective 6 (Par-6), which consistently colocalizes with aPKC in many polarized cell types, including epithelial cells and *Caenorhabditis elegans* one-cell embryos (Hong, 2018; Suzuki and Ohno, 2006). PM/cortical localization of aPKC/Par-6 complex has been assumed mainly based on protein interactions with other polarity proteins such as Bazooka (Baz; Izumi et al., 1998; Krahn et al., 2010; Morais-de-Sá et al., 2010), Crumbs (Crb; Sotillos et al., 2004), Stardust (Sdt/Pals1; Wang et al., 2004), tight junction-associated PDZ protein Patj (Hurd et al., 2003), or Cdc42 (Joberty et al., 2000; Lin et al., 2000; Qiu et al., 2000). Recent studies have delineated some exciting detail mechanisms by which Par-3 and Cdc42 coordinate the spatial and temporal control of aPKC kinase activity during the anterior-posterior (A-P) polarization of worm one-cell embryos (Dickinson et al., 2017; Rodriguez et al., 2017), but how aPKC PM localization and kinase activity are regulated during apical-basal polarization is much less clear. Moreover, in vitro kinase assays yielded conflicting results regarding whether binding of Par-6 to aPKC inhibits or activates its kinase activity (Hong, 2018).

Here we report that the pseudosubstrate region (PSr) of aPKC also functions as a polybasic domain that directly binds to the PM through electrostatic interaction with PM phosphoinositides PI4P and PIP_2. Interestingly, unlike the polybasic domains in Lgl, Numb, and Miranda, PSr in aPKC has not been shown to be phosphorylatable. Instead we show that the PM binding of PSr appears to be allosterically controlled by protein interactions between aPKC and Par-6. Our data suggest a model in which Par-6–dependent allosteric regulation of polybasic PSr in aPKC couples the PM targeting of aPKC and the spatially restricted activation of aPKC kinase during apical-basal polarization.

Results

The conserved PSr is a polybasic domain required for the PM targeting of *Drosophila* aPKC (DaPKC) in *Drosophila* epithelial cells

Our previous studies showed that acute hypoxia induces loss of PM phosphoinositides, which in turn disrupts the PM localization of polybasic domain proteins such as Lgl and Numb in live fly tissues and cultured cells (Dong et al., 2015). Curiously, in the same studies, we found that endogenous DaPKC also showed dramatic loss of PM localization in epithelial cells under hypoxia (Dong et al., 2015), suggesting that PM targeting of DaPKC may be based on direct binding to PM phospholipids. Similar to cPKC and nPKC, aPKC contains a PSr that binds the kinase domain (KD) to induce autoinhibition (Rosse et al., 2010). We identified that the PSr in DaPKC is in fact highly polybasic (Fig. 1 A): the 17-aa PSr contains eight Arg and Lys residues plus one Leu and one Trp residue, and the adjacent 13-aa sequence in C1 domain contains an additional four Arg and Lys residues plus two Phe residues (Heo et al., 2006). Besides the enriched Arg and Lys residues, the presence of Trp, Phe, and Leu is highly indicative of a polybasic domain, as the bulky or long hydrophobic side chains of these residues enhance the PM binding (Heo et al., 2006; McLaughlin and Murray, 2005; Yeung et al., 2006). The PSr is extremely well conserved between DaPKC and mammalian aPKC isoforms PKCζ and PKCι (Fig. 1 A), with a basic-hydrophobic index (Brzeska et al., 2010) of 0.92, comparable to polybasic domains in Lgl (1.00) and Numb (0.89).

Similar to the polybasic domain in Lgl (Dong et al., 2015), PSr in aPKC is capable of direct binding to PI4P and PIP_2 in vitro in liposome pull-down assays. Purified GST fusion of PSr from PKCζ bound PI4P- and PIP_2-containing liposomes, whereas nonpolybasic GST-PSr-KR8Q, with all eight Arg/Lys residues mutated to Gln, did not (Fig. 1 B). PSr is also required for PM targeting of DaPKC in vivo: although ubiquitously expressed aPKC::GFP localized to apical PM in both wild-type and *aPKC*$^{-/-}$ epithelial cells, nonpolybasic aPKC^{KR8Q}::GFP stayed in the cytosol (Figs. 1 C and S1 A).

In vivo, DaPKC::GFP also showed acute and reversible loss from PM, similar to Lgl and Numb in live *Drosophila* follicular and embryonic epithelial cells under hypoxia (Fig. 1 D and Fig. S1 B; and Video 1), consistent with electrostatic binding to phosphoinositides as the primary mechanism targeting DaPKC to the PM. Furthermore, Par-6 is an essential regulatory partner of aPKC and forms a robust complex with aPKC (Hong, 2018; Suzuki and Ohno, 2006). Both proteins are mutually dependent on each other for proper localization and function during cell polarization processes. Consistently, hypoxia in live *Drosophila* follicular and embryonic epithelial cells also induced acute and reversible loss of PM targeting of Par-6::GFP (Fig. 1 D, Fig. S1 B, and Video 2). The loss of DaPKC/Par-6 complex from PM under hypoxia is not due to the concurrent loss of Lgl from PM. Par-6::GFP in *lgl*$^{-/-}$ mutant follicular cells showed expanded localization to basolateral PM but responded to hypoxia identically to Par-6::GFP in wild-type cells (Fig. S1 C). Overall, our data suggest that the polybasic PSr in DaPKC is essential for localizing DaPKC/Par-6 complex to the PM in *Drosophila* epithelia in vivo, likely through direct interaction with PM phosphoinositides such as PI4P and PIP_2 (see below).

PM targeting of mammalian PKCζ depends on both PSr and Par-6

Given the well-documented requirement of Par-6 in aPKC subcellular localization in many cell types (Chen et al., 2018; Hong, 2018; Suzuki and Ohno, 2006), we further investigated the role of Par-6 in regulating the polybasic PSr-mediated PM targeting of aPKC. For this purpose, we took the overexpression approach in nonpolarized HEK293 cells to investigate the potential interactions between aPKC and Par-6 or other exogenously introduced proteins. To keep results consistent, all cultured cell experiments reported here used mammalian proteins of Lgl, aPKC, Par-6, Crb, and Cdc42. The mammalian aPKC family has two isoforms, PKCζ and PKCι, and both contain PSr domains nearly identical to DaPKC's (Fig. 1 A). A PKCζ-specific antibody (Stross et al., 2009) showed that HEK293 cells express no detectable endogenous PKCζ (Fig. 2, A and B) and thus provide a relatively clean background for investigating the PM targeting of the exogenously expressed PKCζ. Surprisingly, we found that PKCζ::GFP was completely cytosolic when expressed alone (Fig. 2 A). However, although Par-6::RFP was

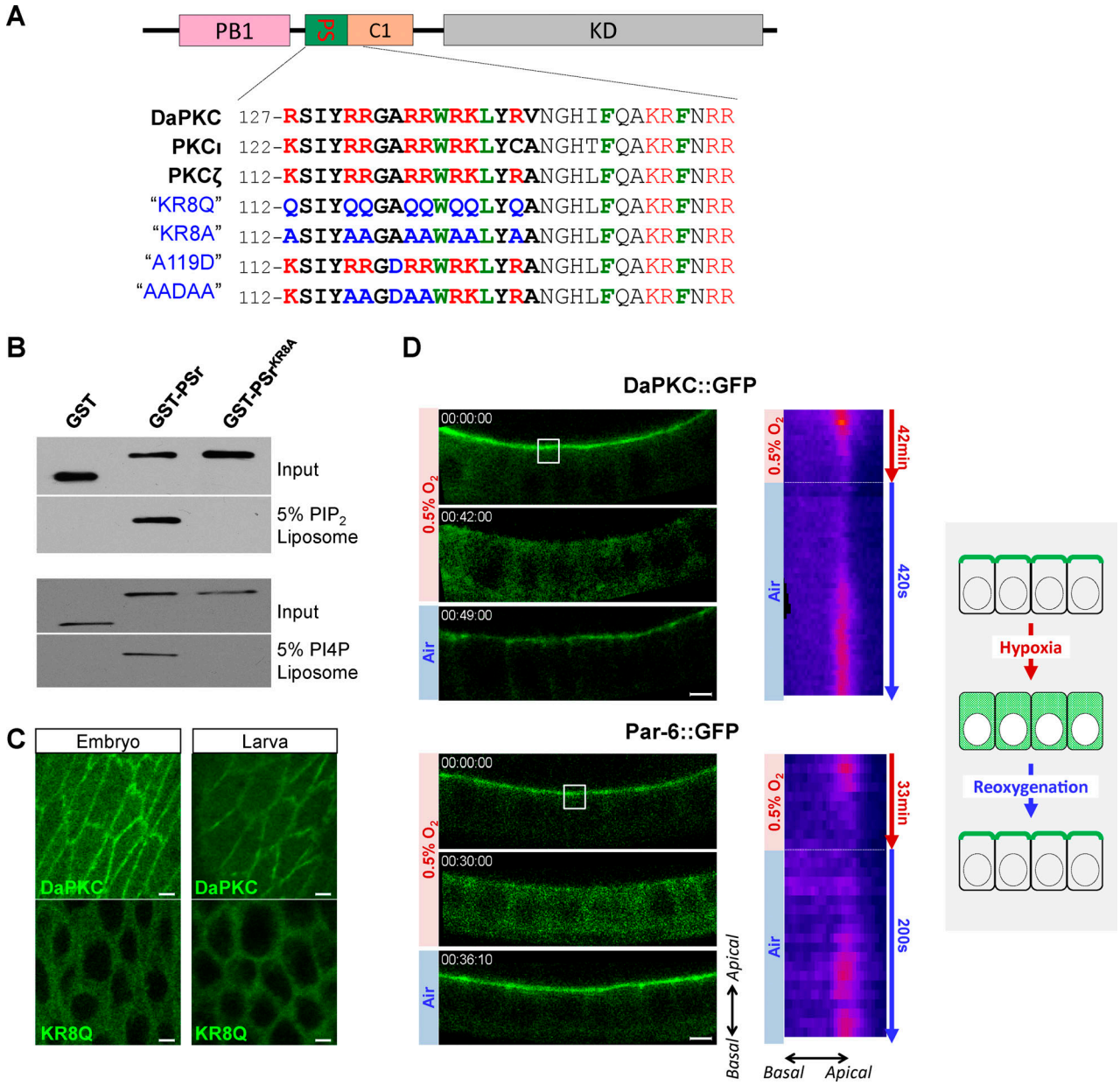

Figure 1. **The conserved polybasic PSr mediates PM targeting of aPKC in *Drosophila* epithelia. (A)** Alignment of the PSr (bold) and adjacent sequences in C1 domain from *Drosophila* and mammalian aPKC isoforms. Sequences are based on NCBI NP_524892.2 (DaPKC), NP_002735.3 (PKCζ), and NP_002731.4 (PKCι). Residues mutated in aPKC^{KR8Q} (KR8Q), aPKC^{KR8A} (KR8A), PKCζ^{A119D} (A119D), and PKCζ^{AADAA} (AADAA) are also shown. **(B)** GST fusion of PSr from PKCζ (GST-PSr), but not the nonpolybasic GST-PSr-KR8A, cosedimented with PI4P- and PIP_2-containing liposomes in vitro. **(C)** DaPKC::GFP (DaPKC), but not nonpolybasic DaPKC^{KR8Q}::GFP (KR8Q), localized to PM in embryonic and larval disc epithelia. **(D)** Follicular epithelial cells in ovaries from *ubi-DaPKC::GFP* or *par-6::GFP* adult females were imaged ex vivo under controlled oxygen environment. Cells are in cross-section view as indicated by the illustration at the far right. PM localization of DaPKC::GFP and Par-6::GFP were acutely inhibited by hypoxia (0.5% O_2) but recovered after reoxygenation by air (see also Videos 1 and 2). Kymographs on the right show the acute loss and recovery DaPKC::GFP or Par-6::GFP on PM during hypoxia and posthypoxia reoxygenation treatments. White boxes indicate where kymographs were sampled. Scale bars: 5 µm (C and D).

also cytosolic when expressed alone, coexpression of PKCζ::GFP and Par-6::RFP resulted in strong and robust PM localization of both proteins (Fig. 2 A). We also made a bicistronic construct that expresses a fusion protein of PKCζ::RFP and Par-6::iRFP connected by a 2A peptide, which self-cleaves during translation (Chan et al., 2011) to produce PKCζ (PKCζ::RFP^{-2A}) and Par-6 ($^{2A-}$Par-6::iRFP) at a constant 1:1 ratio. The fusion protein appeared to be efficiently cleaved (Fig. 2 C), and both PKCζ::RFP^{-2A} and $^{2A-}$Par-6::iRFP showed strong PM localization, as expected (Fig. 2 A).

We confirmed that such colocalization to PM requires direct physical interaction between Par-6 and PKCζ, as a C107Y mutant of PKCζ that specifically abolishes the physical interaction with Par-6 (Kim et al., 2009) failed to localize to PM when coexpressed with Par-6 (Fig. 2, D and E). Furthermore, PM targeting of PKCζ/Par-6 complex requires the polybasic PSr in PKCζ.

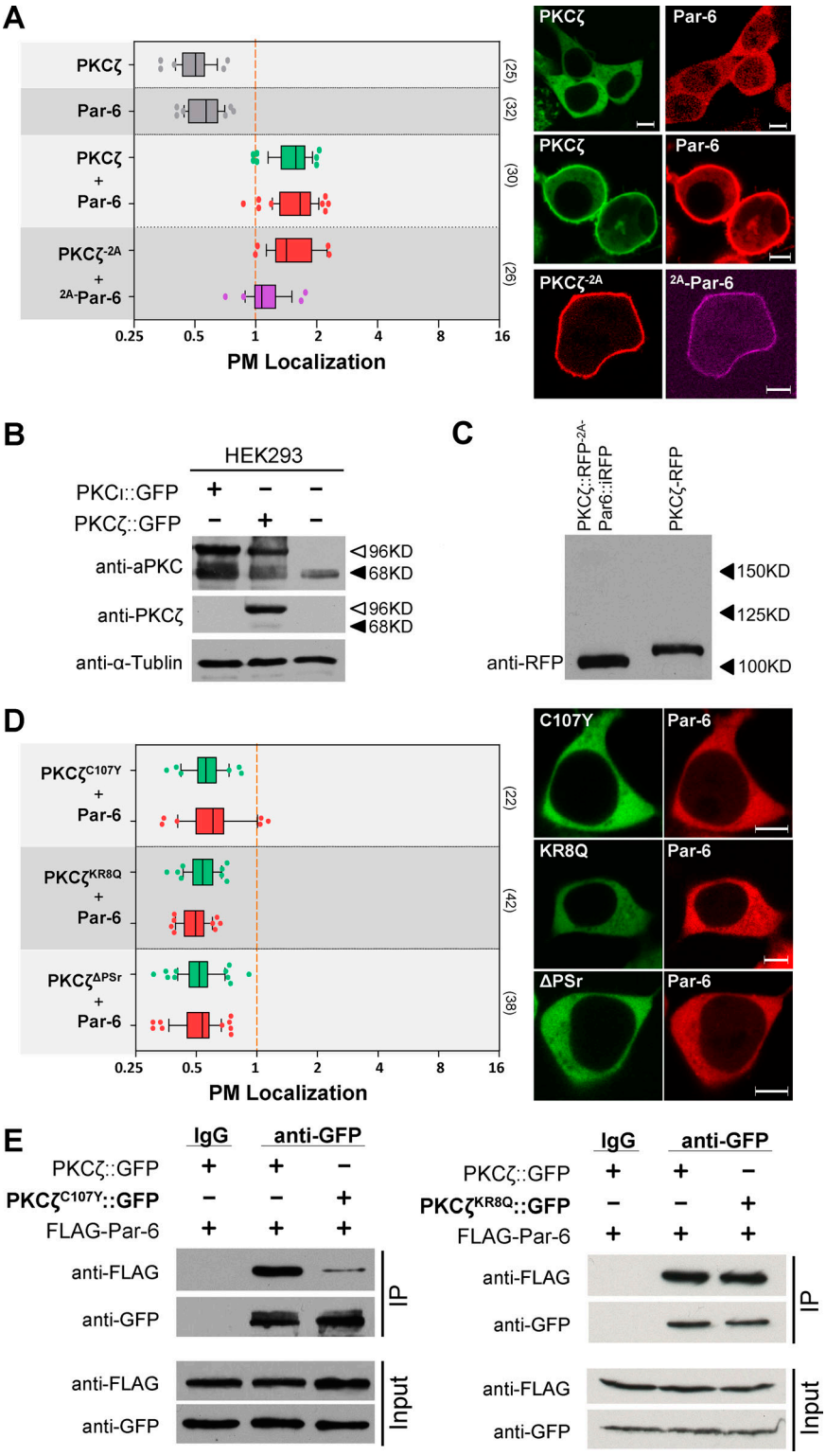

Figure 2. **PM localization of PKCζ in HEK293 cells requires both polybasic PSr and Par-6.** **(A)** PKCζ::GFP or Par-6::RFP was cytosolic when expressed alone, but both became strongly PM-localized when coexpressed. PKCζ::RFP^{-2A} and $^{2A-}$Par-6::iRFP also showed strong PM localization. **(B)** Pan-aPKC antibody (anti-aPKC) detects both exogenously expressed PKC$_L$::GFP and PKCζ::GFP in HEK293 cells (white arrowhead), as well as endogenous expressed aPKC (black arrowhead). PKCζ-specific antibody (anti-PKCζ) specifically detected exogenously expressed PKCζ::GFP but showed no detectable expression of endogenous PKCζ in HEK293. α-Tubulin serves as loading control. **(C)** Only PKCζ::RFP^{-2A} (~100 kD) but not full-length PKCζ::RFP^{-2A-}Par-6::iRFP fusion protein (~150 kD) was detected in cells expressing PKCζ::RFP^{-2A-}Par-6::iRFP. Lysate from cells expressing PKCζ::RFP was loaded and blotted as a positive control. **(D)** PKCζ^{C107Y}::GFP (C107Y), PKCζ^{KR8Q}::GFP (KR8Q), and PKCζ$^{\Delta PSr}$::GFP (ΔPSr) did not localize to PM when coexpressed with Par-6::RFP. **(E)** Both PKCζ::GFP and PKCζ^{KR8A}::GFP, but not PKCζ^{C107Y}::GFP, coimmunoprecipitated with FLAG-Par-6 by anti-GFP antibody from HEK293 cells. In all data plots, boxes extend from 25th and 75th percentiles, with lines in the middle indicating the median and whiskers indicating 10th and 90th percentiles. Sample numbers are indicated in parentheses at the right. Orange dashed lines in quantification figures indicate that the PM localization index = 1 (see Materials and methods). Measurements <1 indicate cytosolic localization, and those >1 indicate PM localization. PM localization axes in all figures are in log2 scale. Scale bars: 5 µm (A and D).

Coexpression of Par-6 with nonpolybasic PKCζ^{KR8Q} resulted in no PM localization of either protein (Fig. 2 D), even though the physical interaction between Par-6 and PKCζ^{KR8Q} remained intact (Fig. 2 E). The loss of PM targeting of PKCζ^{KR8Q} is not due to potential misfolding, as PKCζ^{KR8Q} phosphorylates Lgl similarly to PKCζ in HEK293 cells (Fig. 6, B and C). Our findings are not unique to HEK293 cells, as COS7 and MCF7 breast cancer cells also showed the same Par-6–dependent PM targeting of PKCζ (Fig. S2, A and B). In fully polarized MDCK cells, overexpressed PKCζ alone was cytosolic, although Par-6 alone was partially PM-localized (Fig. S2 C). Nonetheless, coexpression of PKCζ and Par-6 resulted in robust PM localization of both proteins (Fig. S2 C). Interestingly, Par-6 became cytosolic when coexpressed with PKCζ^{KR8Q} (Fig. S2 C), which could indicate a dominant-negative

effect of PKCζ^{KR8Q} due to the formation of PKCζ^{KR8Q}/Par-6 that is incapable of PM targeting. Thus, in polarized MDCK cells, additional mechanisms exist to at least partially target Par-6 to PM, but PM targeting of PKCζ remains dependent on both polybasic PSr and Par-6.

PM targeting of aPKC in HEK293 cells is Cdc42 independent

Cdc42 has been shown to be essential for aPKC/Par-6's localization to anterior PM in *C. elegans* one-cell embryos and has well-characterized physical interactions with Par-6. We thus investigated whether aPKC/Par-6 PM targeting in HEK293 cells is also Cdc42 dependent. In HEK293 cells expressing constitutively active Cdc42^{CA}, Par-6 was readily recruited to the PM, as expected (Fig. 3 A). Furthermore, nonpolybasic PKCζ^{KR8Q} was cytosolic in cells expressing either Cdc42^{CA} (Fig. 3 A) or Par-6 (Fig. 2 D), but became PM-localized in cells coexpressing both Cdc42^{CA} and Par-6 (Fig. 3 A). Thus, in HEK293 cells, the interaction between Cdc42^{CA} and Par-6 is sufficient to recruit Par-6/aPKC complex to the PM, and such PM recruitment can be independent of the polybasic PSr in aPKC. However, the role of Cdc42^{CA} in targeting aPKC/Par-6 is likely context dependent, since in *Drosophila* follicular cells, Cdc42^{CA} overexpression failed to recruit DaPKC^{KR8Q}::GFP to the PM (Fig. 3 B).

In contrast, in HEK293 cells, overexpression of dominant-negative Cdc42^{DN} did not inhibit the PM targeting of aPKC/Par-6 (Fig. 3 A). In *Drosophila* follicular cells subjected to *cdc42-RNAi*, DaPKC::GFP was reduced from PM and enriched at intracellular puncta (Fig. 3 C), likely because of the interaction between aPKC/Par-6 and polarity protein Baz, which was also enriched at the same puncta (Fletcher et al., 2012). To further clarify the role of Cdc42 in our cell-based assays, we made two Par-6 mutants: PB1$^{Par\text{-}6}$, which removes the CRIB and PDZ domains, thus retaining only the N-terminal PB1 domain, and Par-6$^{\Delta PB1}$, which carries the reciprocal truncation. PB1$^{Par\text{-}6}$ was fully capable of targeting PKCζ to PM, but Par-6$^{\Delta PB1}$ was not (Fig. 5 B), suggesting that the physical interaction between the N-terminal PB1 domains in aPKC and Par-6 is sufficient to induce PSr-dependent PM targeting of aPKC. Given that PB1$^{Par\text{-}6}$ does not contain any known Cdc42-interacting domain, PM targeting of PKCζ by PB1$^{Par\text{-}6}$ should be Cdc42 independent. In summary, our results do not exclude the role of Cdc42 in regulating aPKC/Par-6 PM targeting under certain cellular contexts but show that PM targeting of aPKC/Par-6 can be mechanistically independent of Cdc42.

PI4P and PIP_2 act redundantly to target aPKC/Par-6 complex to PM

Phosphoinositides PI4P and PIP_2 are uniquely enriched in PM and are considered the major negatively charged phospholipids responsible for electrostatically binding polybasic domains (Hammond, 2012). To confirm that PM targeting of aPKC/Par-6 complex in cells is indeed mediated by PI4P and PIP_2, we used a well-established system to acutely and selectively deplete PI4P, PIP_2, or both in HEK293. In this inducible system, addition of rapamycin induces dimerization between FK506 binding protein (FKBP)-tagged phosphatases and FKBP-rapamycin binding (FRB)-tagged PM anchor protein Lyn11-FRB-CFP, resulting in acute PM recruitment of phosphatase and concurrent depletion of target phospholipids (Hammond, 2012). In particular, PM recruitment of a chimeric lipid phosphatase Pseudojanin (PJ) rapidly converts both PI4P and PIP_2 in PM to phosphatidylinositol (PI; Hammond, 2012; Fig. 4 A). In HEK293 cells expressing PKCζ::GFP and Par-6::iRFP together with RFP-FKPB-PJ and Lyn11-FRB-CFP, addition of rapamycin induced acute PM localization of PJ and concurrent loss of both PKCζ::GFP and Par-6::iRFP from PM (Fig. 4 B). Depleting either PIP_2 using FKBP-INPP5E or PI4P using FKBP-PJ-Sac induced much milder loss of PM targeting of both proteins (Fig. 4, A and B).

Our data suggest that PI4P and PIP_2 likely act redundantly to bind PKCζ/Par-6 complex to PM. This is in contrast to Lgl, which appears to rely more on PIP_2 for its PM targeting (Dong et al., 2015). Consistently, when we used the similar rapamycin-inducible system to acutely deplete PIP_2 in *Drosophila* follicular epithelial cells, Par-6::GFP remained on the PM (Fig. S3), whereas Lgl::GFP showed significant loss from PM in PIP_2-depleted cells (Dong et al., 2015). We could not carry out assays by inducible depletion of PI4P or both PI4P and PIP_2, as corresponding genetic tools are currently unavailable in *Drosophila*.

Finally, to further confirm the direct binding between aPKC/Par-6 complex and membrane PI4P and PIP_2, we performed liposome binding assays using purified PKCζ, PKCζ/Par-6 complex, or PKCζ^{KR8Q}/Par-6 complex. As shown in Fig. 4 C, purified PKCζ protein alone did not bind PI4P or PIP_2 liposomes, whereas purified PKCζ/Par-6 complex cosedimented with PI4P/PIP_2 liposomes. Furthermore, neither PKCζ^{KR8Q} nor Par-6 showed binding to PI4P/PIP_2 liposomes when purified PKCζ^{KR8Q}/Par-6 was used (Fig. 4 C). Such in vitro data demonstrate that only aPKC/Par-6 complex, but not aPKC alone, can directly bind membrane PI4P and PIP_2 in a polybasic PSr-dependent manner.

PM-binding of PSr in aPKC is likely allosterically regulated by Par-6

Why is PKCζ alone incapable of binding to PM? Previous studies suggested that the PSr in PKCζ binds the kinase domain (KD) to autoinhibit its kinase activity, and that binding of Par-6 likely induces an allosteric conformation change in PKCζ displacing the PSr from the KD (Graybill et al., 2012). We therefore postulate that in unbound aPKC, its PSr is occluded by the KD from binding to the PM but is allosterically exposed once Par-6 binds aPKC. To test this hypothesis, we generated two KD-deletion mutants, PKCζ-ΔKD and PKCζ^{KR8Q}-ΔKD. In contrast to full-length PKCζ, PKCζ-ΔKD localizes to PM in the absence of Par-6, but its PM localization remains dependent on the positive charges of PSr, as nonpolybasic PKC^{KR8Q}-ΔKD is cytosolic regardless the presence of Par-6 (Fig. 5 A). In addition, merely reducing the interaction between PSr and KD is not sufficient to make PSr accessible to PM binding, as two mutants, PKCζ^{A119D} and PKCζ^{AADAA}, carrying previously characterized mutations (Fig. 1 A) shown to reduce the autoinhibition of PSr to the KD (Graybill et al., 2012), were all cytosolic (Fig. 5 A). When coexpressed with Par-6, PKCζ^{A119D} strongly localized to PM (Fig. 5 A), whereas PKCζ^{AADAA} showed barely detectable PM localization, likely because of significantly reduced positive charges of PSr by four Arg→Ala mutations (Fig. 1 A). Finally, expressing Par-6 PB1

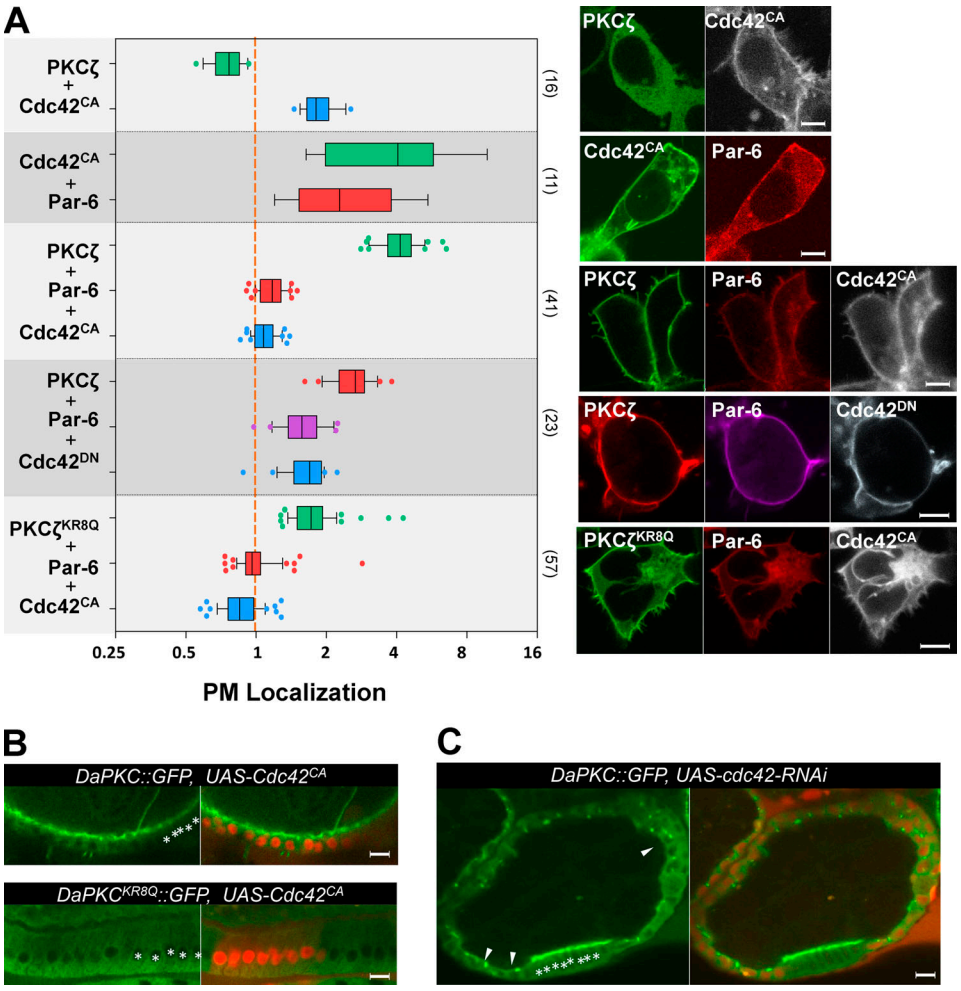

Figure 3. **PM targeting of PKCζ in HEK293 cells is independent of Cdc42. (A)** PKCζ::GFP was cytosolic when coexpressed with BFP::Cdc42^{CA}. Par-6::RFP localized to PM in cells coexpressing GFP::Cdc42^{CA}. Coexpressed PKCζ and Pra-6 were PM-localized in cells expressing either BFP::Cdc42^{CA} or BFP::Cdc42^{DN}. Nonpolybasic PKCζ^{KR8Q}::GFP was PM-localized in cells expressing both BFP::Cdc42^{CA} and Par-6::RFP. **(B)** Overexpression of Cdc42^{CA} did not change DaPKC::GFP and DaPKC^{KR8Q}::GFP subcellular localization in *Drosophila* follicular epithelial cells. **(C)** DaPKC::GFP formed intracellular puncta (arrowheads) in *cdc42-RNAi* follicular cells. In B and C, cells expressing *UAS-cdc42-RNAi* or *UAS-Cdc42^{CA}* are marked by RFP expression. Asterisks highlight wild-type cells. Scale bars: 5 µm (A and B); 15 µm (C).

domain (PB1^{Par-6}), but not Par-6$^{\Delta PB1}$, induced PM localization of both PKCζ and PB1^{Par-6} (Fig. 5 B), suggesting that interaction between PKCζ and Par-6 PB1 domain alone is both sufficient and necessary to target PKCζ to PM. Although the lack of full protein structures of aPKC and Par-6 makes it difficult to conduct comprehensive structure-based experiments to further confirm the allosteric regulation of PSr by Par-6, our data strongly support a model that PB1/PB1 interaction between aPKC and Par-6 is both sufficient and necessary to allosterically displace the polybasic PSr from KD in aPKC, exposing PSr to electrostatic binding to the PM.

Par-6–dependent PM targeting inhibits PKCζ kinase activity

Binding of Par-6 is considered an essential step in regulating the kinase activity of aPKC, although whether Par-6 activates or inhibits aPKC remains unsettled and may well depend on additional regulators presented in different cell types (Hong, 2018). To investigate how Par-6 regulates PKCζ activity in vivo, we established aPKC kinase activity assays in HEK293 cells based on the loss of Lgl PM localization that serves as a sensitive, robust, and quantifiable readout for measuring aPKC phosphorylation of Lgl in live cells. When expressed alone in HEK293 cells, mammalian Lgl::GFP showed consistently strong and robust PM localization (Fig. 6 A) that was strongly reduced in cells expressing PKCζ but not kinase-dead PKCζ^{K281W} (Fig. 6 A). An anti-phospho-Lgl antibody confirmed the phosphorylation of Lgl in HEK293 cells coexpressing PKCζ (Fig. 6 C), suggesting that overexpressed PKCζ alone contains basal kinase activity sufficient to phosphorylate Lgl, consistent with the fact that in vitro purified aPKC has ∼10% of activated kinase activity (Zhang et al., 2014). To further confirm that the loss of Lgl PM localization is due to the phosphorylation by PKCζ, we generated a nonphosphorylatable Lgl^{S6A}::GFP in which all six conserved phospho-serines were mutated to alanine. As expected, Lgl^{S6A}::GFP remained on the PM when coexpressed with PKCζ (Fig. 6 A).

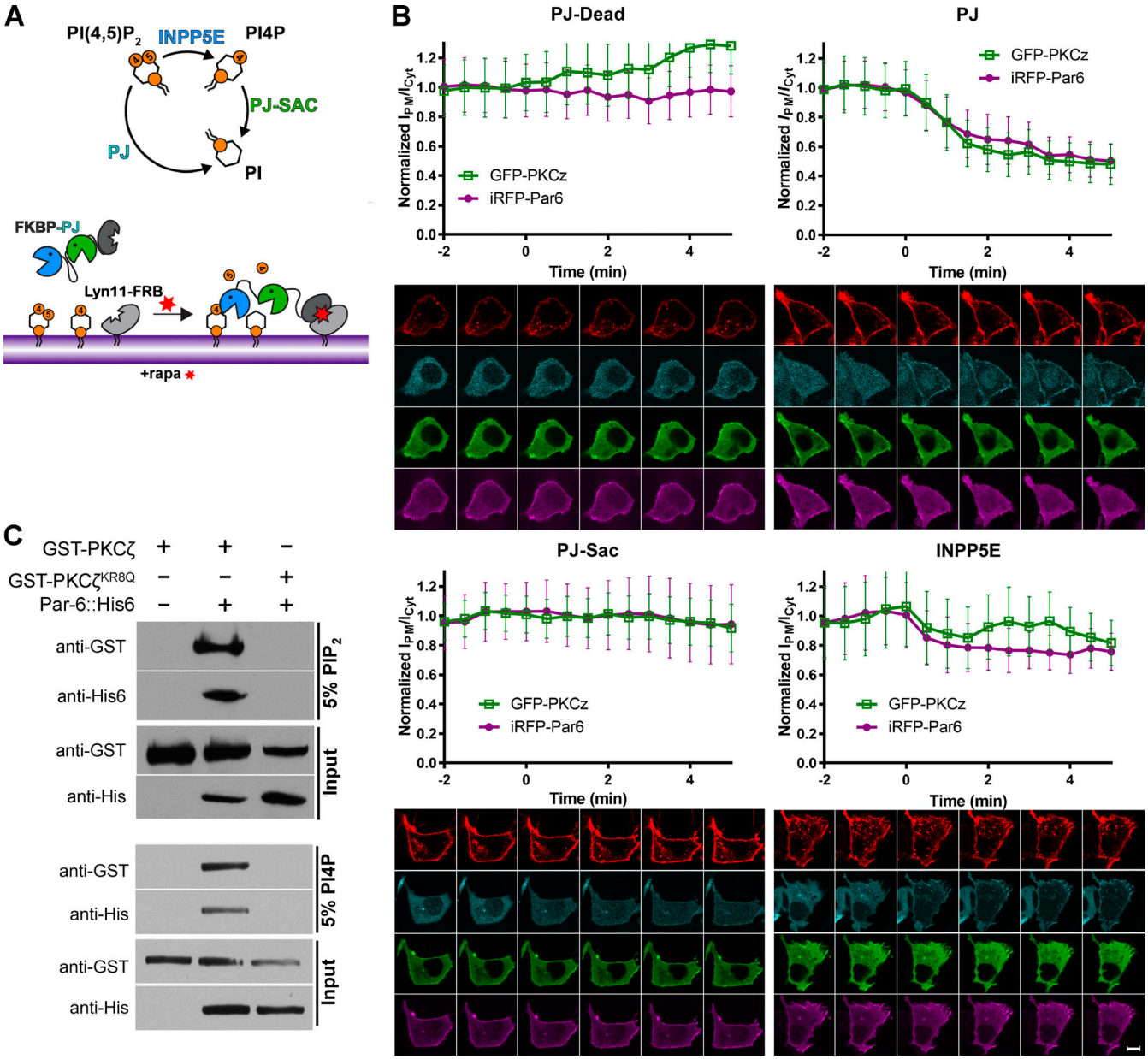

Figure 4. **PM targeting of PKCζ and Par-6 depends on both PI4P and PIP_2. (A)** INPP5E converts PIP_2 to PI4P, which can be further converted to PI by Sac, whereas PJ converts both PIP_2 and PI4P to PI. Box: FKBP-PJ can be acutely recruited to PM through rapamycin (rapa)-induced heterodimerization with PM-anchored Lyn11-FRB. PM recruitment of PJ results in acute depletion of both PI4P and PIP_2. **(B)** PM localization of PKCζ::GFP and Par-6::iRFP was quantified before and after rapamycin addition in HEK293 cells expressing Lyn11-FRB-CFP and mCherry-FKBP-PJ, -Sac, -INPP5E, or -PJ-dead (as a negative control). Representative time-lapse images of Lyn11-FRB-CFP (red), PKCζ::GFP (green), Par-6::iRFP (magenta), and mCherry-FKBP-PJ/Sac/INPP5E/PJ-dead (cyan) are shown under each quantification figure. For each quantification, means ± SEM from 20–30 cells pooled across three independent experiments were plotted. **(C)** Purified GST-PKCζ/Par-6::His6 complex, but not purified GST-PKCζ alone or GST-$PKC\zeta^{KR8Q}$/Par-6::His6 complex, bound to PI4P- and PIP_2-liposomes. Scale bars: 5 µm (B, all panels).

We then tested the kinase activity of PM-targeted aPKC/Par-6 complex. Strikingly, in HEK293 cells coexpressing Lgl::GFP, PKCζ::RFP, and Par-6::iRFP, all three proteins were strongly PM-localized (Fig. 6 A), and anti-phospho-Lgl antibody failed to detect phosphorylation on Lgl (Fig. 6 C). Similar results were also seen in cells expressing Lgl::GFP and PKCζ::RFP^{-2A}-Par-6::iRFP (Fig. 6 A). Thus, binding of Par-6 not only targets PKCζ to PM, but also appears to strongly inhibit its kinase activity. This apparent inhibition of PKCζ kinase activity by Par-6 is not due to the PM localization of PKCζ alone, as we made a Lyn11-PKCζ that contains the constitutive PM-binding domain Lyn11 and found that it also strongly delocalized Lgl::GFP to the cytosol and was efficiently inhibited by Par-6 (Fig. 6, B and C). We also compared the Par-6 inhibition on cytosolic $PKC\zeta^{KR8Q}$ and PM-bound Lyn11- $PKC\zeta^{KR8Q}$. Both kinases strongly reduced the PM localization of Lgl and were similarly inhibited by Par-6 (Fig. 6, B and C), suggesting that PM localization of PKCζ is not required for the kinase inhibition by Par-6.

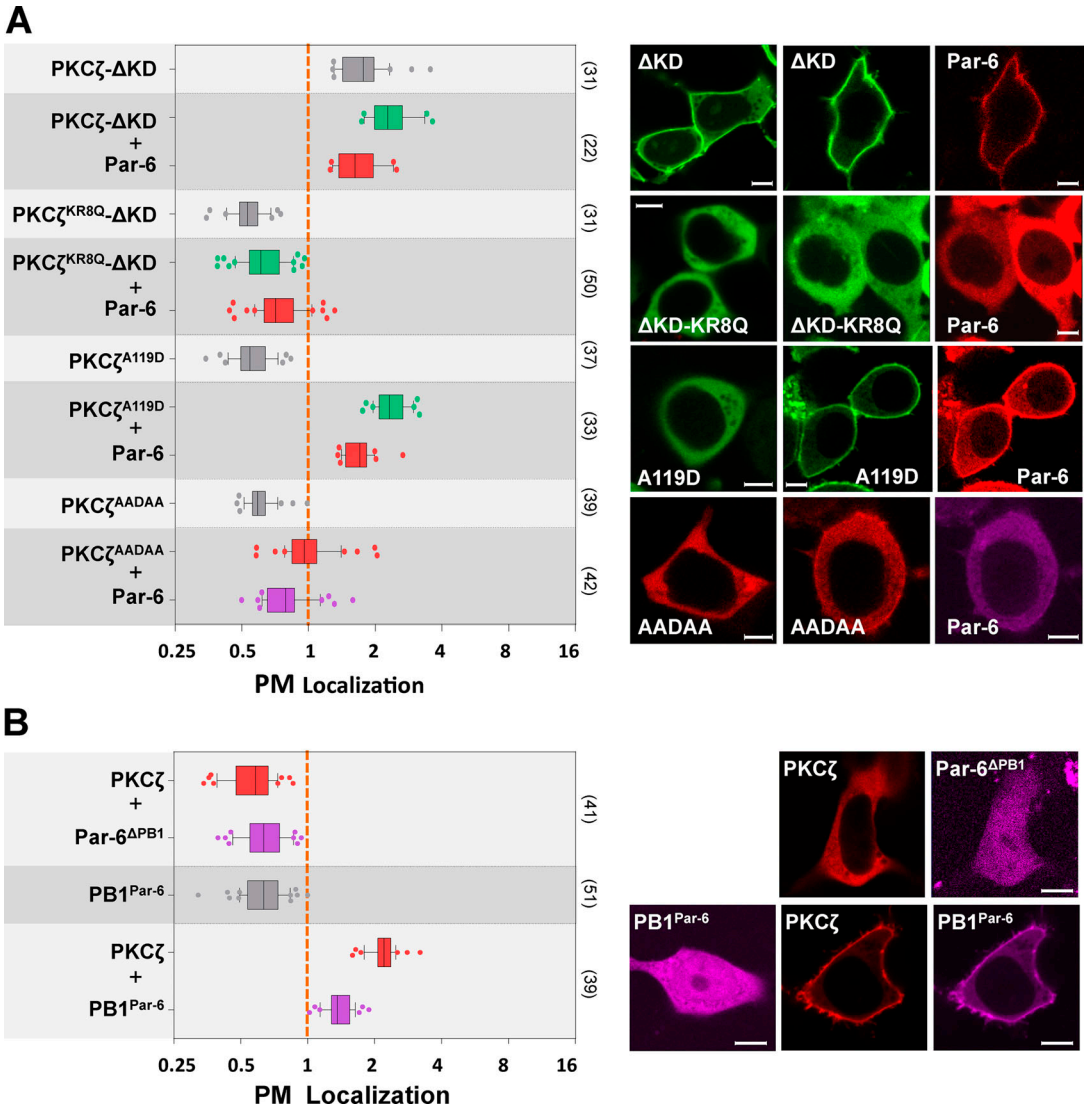

Figure 5. **Par-6 interaction with PKCζ is required for polybasic PSr to bind PM. (A)** PKCζ-ΔKD::GFP (ΔKD) localized to PM with or without the coexpression of Par-6::RFP. PKCζ-ΔKD^{KR8Q}::GFP (ΔKD-KR8Q) was cytosolic with or without the coexpression of Par-6::RFP. PKCζ^{A119D}::GFP (A119D) and PKCζ^{AADAA}::GFP (AADAA) were cytosolic when expressed alone. When coexpressing with Par-6::RFP, PKCζ^{A119D}::GFP was strongly PM-localized, whereas PKCζ^{AADAA}::GFP was barely PM-localized. **(B)** PKCζ::RFP and Par-6$^{\Delta PB1}$::iRFP remained in cytosol when coexpressed. PB1^{Par-6}::iRFP was cytosolic when expressed alone, but when coexpressed with PKCζ::RFP, both became PM-localized. All experiments were performed in HEK293 cells. Scale bars: 5 µm.

Curiously, in polarized MDCK cells, overexpressed PKCζ failed to dislocalize Lgl::GFP from PM (Fig. S4 B), suggesting that Lgl phosphorylation by aPKC is tightly controlled by additional mechanisms. Nonetheless, our results in nonpolarized HEK293 cells suggest that binding of Par-6 not only targets aPKC to the PM but also inhibits its kinase activity.

Crb activates aPKC/Par-6 kinase activity to phosphorylate Lgl

The PB1 domain of Par-6 alone (PB1^{Par-6}) was capable of targeting PKCζ to PM (Fig. 5 B), but it did not inhibit the phosphorylation of Lgl::GFP by PKCζ (Fig. 7 A), nor did Par-6ΔPDZ, in which the C-terminal PDZ domain was deleted (Fig. 7 A). Such results suggest that the PDZ domains or the C-terminus of Par-6 could be specifically required for inhibiting PKCζ kinase activity on Lgl (Fig. 7 A), which is consistent with the finding that overexpression of Par-6 C-terminus inhibits PKCι/λ activity in MDCK cells (Kim et al., 2007). The C-terminus of Par-6 interacts with multiple proteins, including activated Cdc42, which binds the Par-6 CRIB domain and moderately activates kinase activity of aPKC/Par-6 complex in vitro (Yamanaka et al., 2001). However, PM localization of Lgl::GFP remained high in HEK293 cells expressing Cdc42^{CA}, PKCζ, and Par-6 (Fig. 7 B), suggesting that Cdc42^{CA} is not sufficient to activate aPKC in our cell-based assays. Our results are consistent with genetic evidences that *Drosophila* Cdc42 is not required for aPKC to phosphorylate Lgl (Hutterer et al., 2004) and Baz (Walther and Pichaud, 2010) in vivo.

Besides Cdc42, apical polarity protein Crb also interacts with Par-6. Crb is a transmembrane protein, and the C-terminus of its intracellular domain is a PDZ-binding domain (PBD) that can bind the PDZ domain in Par-6 (Kempkens et al., 2006). We

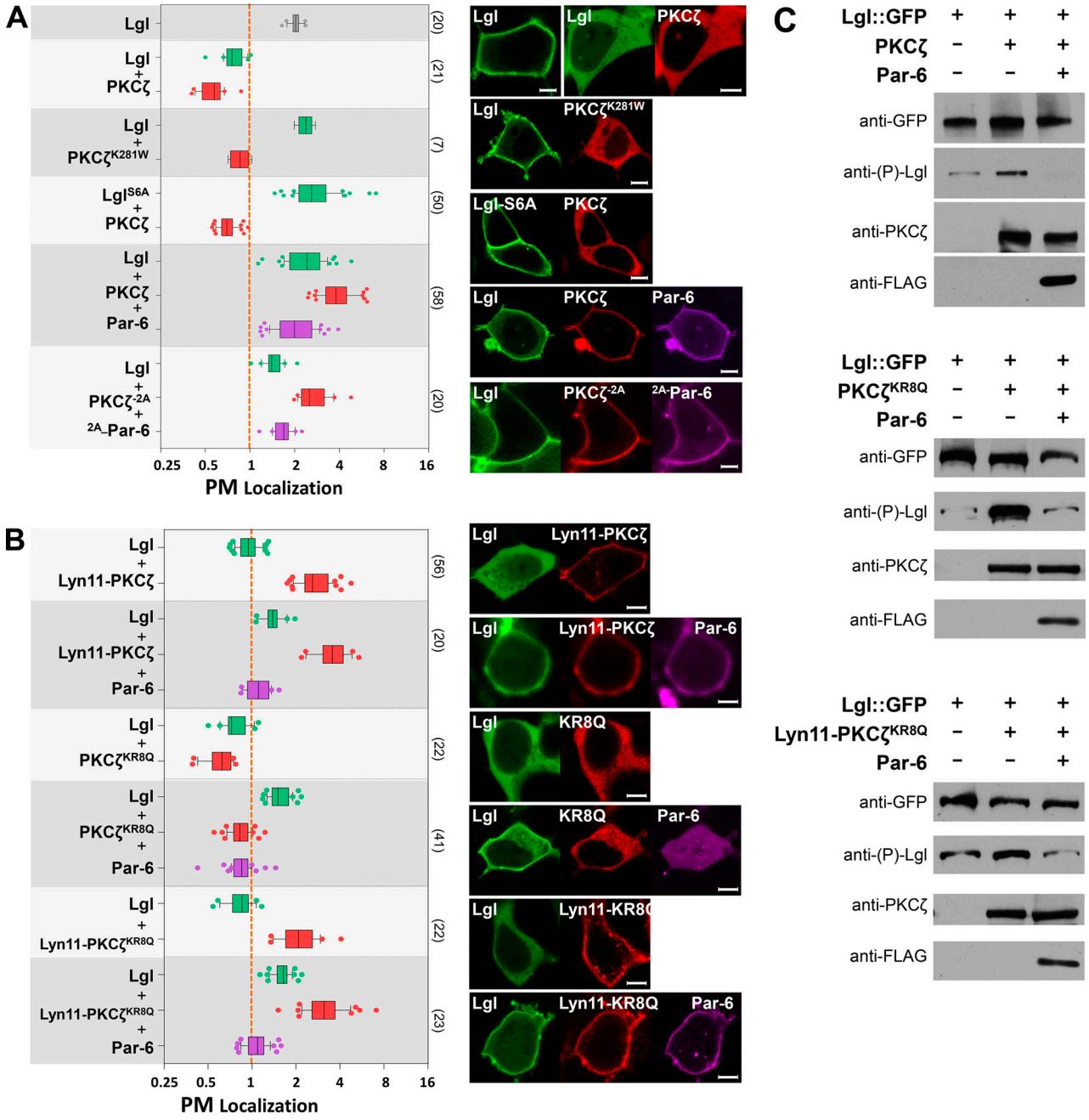

Figure 6. **PM-targeted PKCζ/Par-6 complex is inhibited from phosphorylating Lgl. (A)** PM localization of Lgl::GFP was strongly reduced in cells expressing PKCζ::RFP but not kinase-dead PKCζ^{K281W}::RFP. Nonphosphorylatable Lgl^{S6A}::GFP remained PM-localized in cells expressing PKCζ::RFP. Lgl::GFP remained PM-localized in cells coexpressing PKCζ::RFP and Par-6::iRFP. Lgl::GFP also showed strong PM localization in cells expressing PKCζ::RFP^{-2A-}Par-6::iRFP. **(B)** PM localization of Lgl::GFP was strongly reduced in cells expressing Lyn11-PKCζ::RFP, PKCζ^{KR8Q}::RFP (KR8Q), and Lyn11-PKCζ^{KR8Q}::RFP (Lyn11-KR8Q). In all three cases, coexpression of Par-6::iRFP increased PM localization of Lgl::GFP. **(C)** Cells expressing Lgl::GFP only, expressing both Lgl::GFP and PKCζ::RFP (or PKCζ^{KR8Q}::RFP or Lyn11-PKCζ^{KR8Q}::RFP), or expressing Lgl::GFP together with PKCζ::RFP (or PKCζ^{KR8Q}::RFP or Lyn11-PKCζ^{KR8Q}::RFP) and FLAG::Par-6, were directly lysed in SDS loading buffer and analyzed by Western blot. Anti-(P)-Lgl, antibody against phosphorylated Lgl. All experiments were performed in HEK293 cells. Scale bars: 5 µm.

therefore investigated whether Crb could directly activate the kinase activity of aPKC/Par-6 complex through its interaction with the Par-6 PDZ domain. Par-6 became localized to the PM in HEK293 cells expressing membrane-bound Crb intracellular domain (Crb-intra) but not Crb-intra$^{\Delta ERLI}$, in which the C-terminal PBD was deleted, confirming that Par-6 binds to the PBD of Crb-intra (Fig. S4 A). Moreover, in HEK293 cells expressing aPKC and Par-6 together with Crb-intra but not Crb-intra$^{\Delta ERLI}$, Lgl::GFP was strongly reduced from the PM (Fig. 7 B). The loss of Lgl::GFP from PM in cells expressing Crb-intra, aPKC, and Par-6 is phosphorylation dependent, as nonphosphorylatable Lgl^{S6A}::GFP remained on PM in these cells (Fig. 7 B). Lgl::GFP

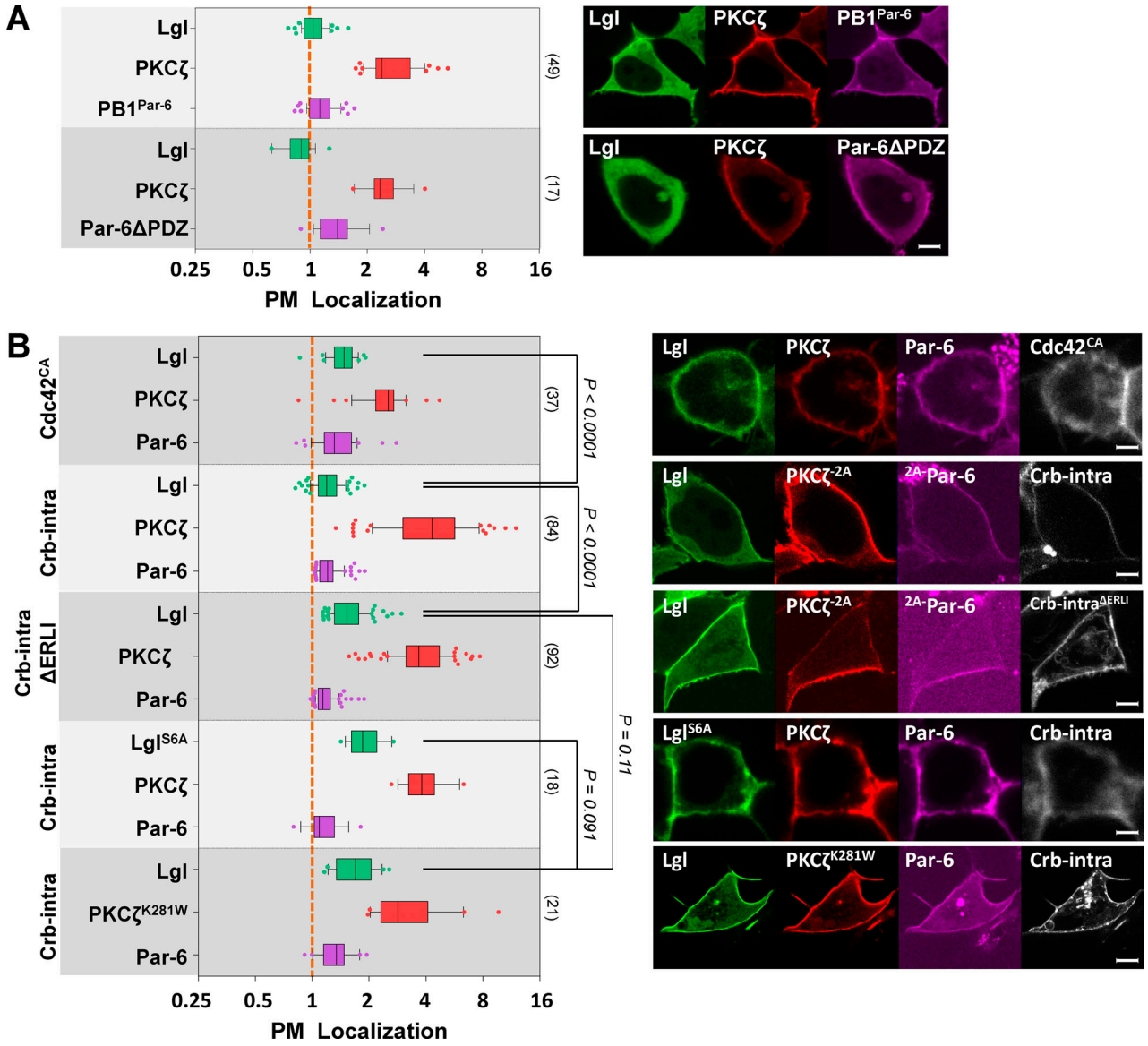

Figure 7. **Crb-intra activates PM-targeted aPKC/Par-6 complex. (A)** In HEK293 cells expressing either PB1^{Par-6}::iRFP or Par-6ΔPDZ::iRFP, PKCζ::RFP was strongly PM-localized, whereas Lgl::GFP was strongly reduced from PM. **(B)** In HEK293 cells expressing Lgl::GFP, PKCζ::RFP, and Par-6::iRFP, PM localization of Lgl::GFP was strongly reduced when BFP::Crb-intra, but not BFP::Crb-intra$^{\Delta ERLI}$ or BFP::Cdc42^{CA}, was coexpressed. Lgl^{S6A}::GFP remained on PM in cells expressing PKCζ::RFP, Par-6::iRFP, and BFP::Crb-intra. Lgl::GFP remained on PM in cells expressing BFP::Crb-intra, Par-6::iRFP, and kinase-dead PKCζ^{K281W}::RFP. Scale bars: 5 µm.

also maintained PM localization in cells expressing Crb-intra, Par-6, and kinase-dead aPKC^{K281W} (Fig. 7 B). These results support a model in which direct interaction between Crb-intra and Par-6 in a PM-bound aPKC/Par-6 complex activates aPKC kinase activity.

Consistent with our cell-based assays, overexpression of Crb in *Drosophila* follicular cells and embryonic epithelial cells expanded Crb and DaPKC into basolateral PM and strongly delocalized Lgl::GFP, but not nonphosphorylatable Lgl^{S5A}::GFP, from basolateral PM (Fig. 8, A–C). The loss of Lgl::GFP from PM in Crb-overexpressing cells was completely reversed when DaPKC or Par-6 was also knocked down by RNAi (Fig. 8, E and F). Furthermore, the loss of PM Lgl::GFP in Crb-overexpressing cells is comparable to cells overexpressing DaPKC-ΔN, which is considered fully activated owing to the deletion of the N-terminus including PSr (Betschinger et al., 2003; Fig. 8 G). Thus, in Crb-overexpressing follicular cells, DaPKC is the key kinase phosphorylating Lgl and is likely highly activated. In contrast, in *Drosophila crb*$^{-/-}$ embryos, DaPKC also extended to the basolateral PM but Lgl remained on PM (Fig. 8 D), suggesting that Crb is necessary to promote DaPKC phosphorylation on Lgl in embryonic epithelial cells in vivo.

Discussion

Electrostatic binding to phosphoinositides by polybasic PSr targets aPKC to PM

In this study, we show that the PSr in aPKC is a typical polybasic domain capable of directly targeting aPKC to PM via its electrostatic

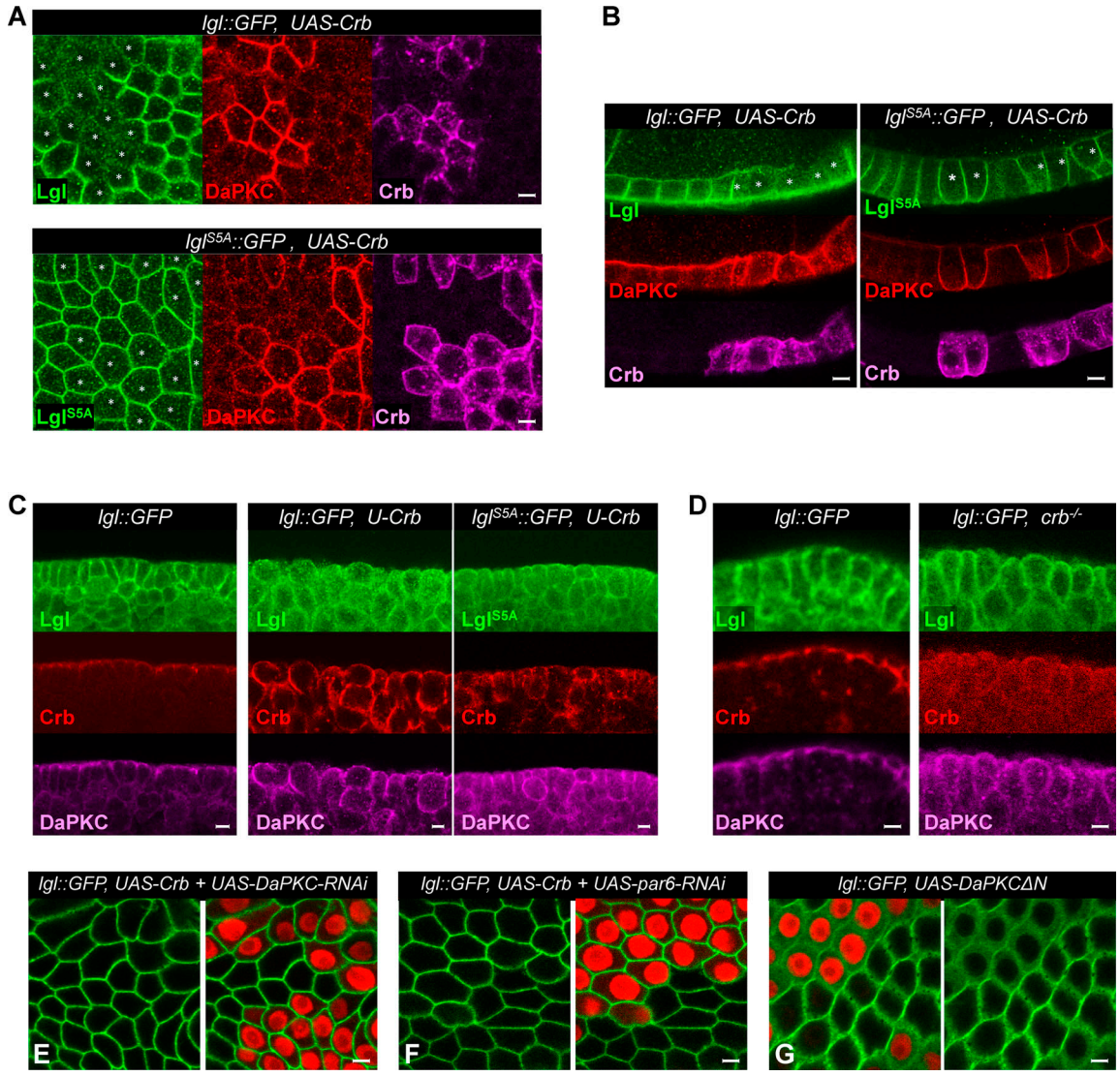

Figure 8. **Crb promotes DaPKC phosphorylation on Lgl in vivo. (A and B)** *Drosophila lgl::GFP* or lgl^{S6A}*::GFP* follicular epithelial cells overexpressing Crb were immunostained for GFP (green), DaPKC (red), and Crb (magenta). Images in A are in tangential view and were sectioned below the apical surface of follicular cells where Crb and aPKC normally are absent. Images in B are in cross section view of follicular epithelial cells, showing overexpressed Crb expanded into the lateral PM along with DaPKC. Cells overexpressing Crb are highlighted by asterisks in green-channel images. **(C)** Wild-type *lgl::GFP* embryos and embryos of *lgl::GFP UAS-Crb/Mat-Gal4* or lgl^{S5A}*::GFP UAS-Crb/Mat-Gal4* were immunostained for GFP (green), Crb (red), and aPKC (magenta). All embryonic epithelial cells were in cross-section view. Note the loss of Lgl::GFP, but not Lgl^{S5A}::GFP, from the PM under Crb overexpression driven by *Mat-Gal4* (see Materials and methods). **(D)** Wild-type *lgl::GFP* embryos and *lgl::GFP; crb*$^{-/-}$ mutant embryos were immunostained for GFP (green), Crb (red), and aPKC (magenta). In *crb*$^{-/-}$ embryos, red channel was overexposed to confirm no detectable expression of Crb. In *crb*$^{-/-}$ embryonic epithelial cells, both Lgl and DaPKC became localized all around PM. **(E and F)** Lgl::GFP remained on PM in Crb-overexpressing cells that also expressed *DaPKC-RNAi* (E) or *par-6-RNAi* (F). **(G)** Lgl::GFP was severely lost from PM in follicular cells expressing DaPKCΔN. In E–G, cells expressing *DaPKC-RNAi*, *par-6-RNAi* or DaPKCΔN are marked by RFP expression (see Materials and methods). Scale bars: 5 µm.

interaction with negatively charged phosphoinositides PI4P and PIP_2 in PM. This is in contrast to the assumption that protein–protein interactions are solely responsible for localizing aPKC to PM or cell cortex. In addition, unlike phosphorylatable polybasic domains in Lgl, Numb, and Miranda, the polybasic PSr in aPKC has not been shown to be phosphorylatable. Instead, we report a novel example of a potential allosteric regulation of a polybasic domain for PM binding. As illustrated in Fig. 9, our data support a model in which the polybasic PSr in unbound aPKC is occluded by the KD from binding PM, whereas the binding of Par-6 to aPKC via PB1 domains induces potential conformational changes in aPKC that make the polybasic PSr accessible to PM binding.

Cdc42 plays an important role in mediating the PM targeting of aPKC/Par-6 in certain cell types such as *C. elegans* one-cell embryos, and we found that activated Cdc42 binds Par-6, which in turn can recruit nonpolybasic $aPKC^{KR8Q}$ to the PM in HEK293 cells. However, our in vitro and in vivo studies suggest that electrostatic binding to PI4P and PIP_2 alone can be sufficient to localize aPKC/Par-6 complex to the PM. Our results are consistent

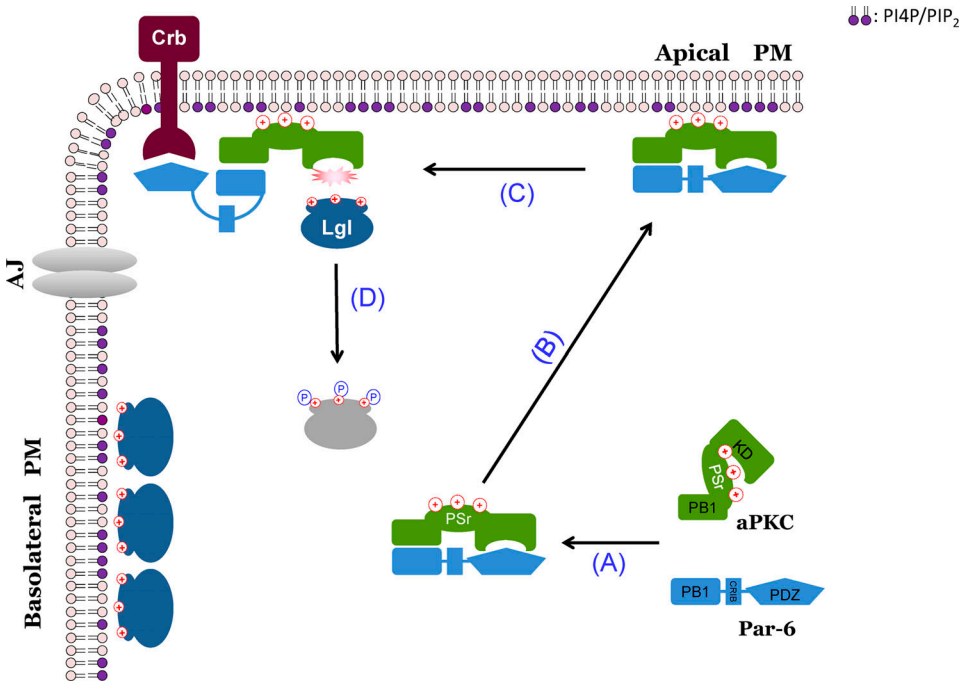

Figure 9. **A hypothetic model of aPKC PM targeting and kinase activation. (A)** Free cytosolic aPKC in autoinhibited conformation has polybasic PSr blocked by the KD from binding to PM. Binding of Par-6 to aPKC induces conformation changes that expose the PSr in aPKC and allow the C-terminus of Par-6 to simultaneously inhibit the aPKC KD. **(B)** Polybasic PSr in aPKC/Par-6 complex binds to PM via electrostatic interaction with PI4P and PIP_2, which are uniquely enriched on PM. **(C)** Intracellular domain of apical polarity protein Crb interacts with the C-terminal PDZ domain of Par-6 and releases its inhibition on aPKC KD. Interaction with Crb could also facilitate the apical enrichment of PM-bound aPKC/Par-6 in cells. **(D)** Activated aPKC phosphorylates Lgl to prevent it from binding to apical PM. Illustration is based on *Drosophila* epithelial cells. AJ, adherens junction.

with findings that removing Cdc42 in *C. elegans* late embryos or in *Drosophila* pupal epithelial cells does not severely disrupt aPKC and Par-6 localization (Georgiou et al., 2008; Zilberman et al., 2017). Whereas Cdc42 directly regulates aPKC/Par-6 PM targeting under certain cellular contexts, our results demonstrate a PM-targeting mechanism of aPKC/Par-6 that is mechanistically independent of Cdc42 or other aPKC/Par-6 interacting proteins.

Our hypoxia assay suggests that, at least in *Drosophila* follicular and embryonic epithelial cells, binding to PI4P and PIP_2 is likely the primary mechanism localizing aPKC/Par-6 to the PM in vivo. In these cells, the Par-6–dependent electrostatic binding to PM by PSr likely functions as the first step to localize aPKC/Par-6 to the PM, followed by further enrichment to specific membrane domains such as apical PM through protein–protein interactions with, for instance, apical Crb complex. Thus, while mechanisms governing the aPKC/Par-6 subcellular localization can be heavily cell type specific and multilayered, our results highlight that the electrostatic PM-binding property of aPKC needs to be taken into consideration when studying the protein regulators of aPKC/Par-6 subcellular localization.

Our studies also suggest potential new negative regulators that may act specifically at the electrostatic interaction to prevent aPKC from binding to the PM, by mechanisms such as masking the PSr, inhibiting the allosteric changes induced by Par-6, or sequestering the phospholipids in the PM. Moreover, it is notable that a PI4P- and PIP_2-dependent mechanism makes aPKC PM targeting vulnerable to stress conditions such as hypoxia and ATP inhibition that deplete these phospholipids in the PM (Dong et al., 2015). The acute and reversible loss of PM targeting of polybasic polarity proteins such as Lgl, aPKC, and Par-6 may have profound implications in epithelial cells for maintaining and restoring their apical-basal polarity when undergoing hypoxia, ischemia, and reperfusion.

Par-6 controls both aPKC PM targeting and kinase activity

Mechanisms coupling the aPKC kinase activity with its subcellular localization are essential for aPKC to phosphorylate targets at the right place and right time (Hong, 2018), but molecular details about these mechanisms remain largely elusive. Recent studies began to reveal exciting details on how aPKC/Par-6 kinase activity and subcellular localization can be regulated by the clustering of Par-3(Baz) and diffusive interactions with Cdc42 (Dickinson et al., 2017; Rodriguez et al., 2017), but these studies so far have been limited to the process of A-P polarization in worm one-cell embryos. Here we show that, in *Drosophila* epithelial cells and cultured mammalian cells, the electrostatic binding of aPKC to PM alone may provide a mechanism for Par-6 to play a pivotal role in coupling the PM targeting and control of kinase activity of aPKC (Fig. 9). It is possible that conformational changes in aPKC induced by Par-6 may not only expose PSr to PM binding but also allow the C-terminus of Par-6 to simultaneously inhibit aPKC's KD. More experiments, however, are needed to further validate this hypothesis.

Our allosteric model is based on previous studies suggesting the displacement of PSr from aPKC upon binding of Par-6 (Graybill et al., 2012). However, in that study, Par-6 appears to

activate aPKC in vitro and in *Drosophila* S2 cells. Such a discrepancy could be because S2 cells already express proteins capable of releasing the inhibition of Par-6 on aPKC. It should be noted that studies from multiple groups yielded conflicting results on whether Par-6 inhibits or activates aPKC kinase activity (Atwood et al., 2007; Chabu and Doe, 2008; Graybill et al., 2012; Lin et al., 2000; Yamanaka et al., 2001). Most of these studies relied on immunoprecipitated or reconstituted aPKC/Par-6 complex to measure the kinase activity in solution in vitro. Given that the majority of aPKC substrates are PM-bound polybasic domain–containing proteins, it might be critical to assay aPKC/Par-6 kinase activity in its PM-bound form in live cells.

In addition, it is conceivable that binding to PM may physically shield the polybasic domain in a target protein from being accessible to aPKC, as suggested by the increased resistance of membrane-bound Lgl to aPKC phosphorylation in vitro (Visco et al., 2016). This is consistent with our finding that phosphorylation of Lgl appears to be inhibited when both Lgl and aPKC/Par-6 complex are electrostatically attached to PM. On the other hand, the transient and dynamic nature of lipid binding by polybasic domains (Hammond et al., 2009) could also effectively enrich a local cytosolic pool of target proteins near PM, which works in favor of PM-bound aPKC to encounter its substrates. Such intricate relationships between PM targeting and aPKC phosphorylation of polybasic polarity proteins remain to be further explored.

PM targeting and spatial control of aPKC kinase activation

Similar to cPKC and nPKC, the electrostatic binding of PSr to PM could potentiate the kinase activity of aPKC/Par-6 complex by further preventing PSr from autoinhibiting the KD (Rosse et al., 2010; Garg et al., 2014). This is supported by in vitro studies showing that Par-6 binding to aPKC inhibits its kinase activity but also potentiates its activation upon subsequent molecular events (Yamanaka et al., 2001). PM-bound aPKC/Par-6 complexes with inhibited but potentiated kinase activity are ideal targets for additional activation to fine-tune aPKC localization and kinase activity. Curiously, we found that Cdc42 did not activate PM-bound aPKC/Par-6 to phosphorylate Lgl in our cultured cell assays, but interaction between Par-6 and apical transmembrane protein Crb reversed Par-6's inhibition on aPKC kinase activity. Supporting the role of Crb in enriching and activating aPKC/Par-6, Crb colocalizes with aPKC/Par-6 complex and is required for enriching the aPKC/Par-6 complex to the apical PM in fly embryonic epithelial cells and in many specialized membranes in *Drosophila*, including apical membranes of photoreceptors (Hong et al., 2003; Pellikka et al., 2002) and lumens in scolopale cell in chondotoral organs (Y. Hong, unpublished data). However, Crb is not required for apical enrichment of aPKC in follicular cells (Sherrard and Fehon, 2015); therefore, additional proteins besides Crb must be responsible for the apical enrichment and activation of aPKC/Par-6 in different types of epithelial cells.

It is of note that our studies are primarily based on cultured cells and limited cell types of *Drosophila* epithelial cells, and thus present a simplified model regarding the relationships between aPKC/Par-6 and its regulators. Our data do highlight that aPKC/Par-6 activity can be regulated by multiple regulators such as PM phosphoinositides, Cdc42, and Crb under different cellular and polarity contexts. Extrapolating our study to further investigate the role of aPKC in regulating cell polarity requires experiments to take into account the more complicated cellular contexts in different cell types.

Materials and methods

Fly stocks and genetics

The following *Drosophila* stocks were used in this study: knockout alleles of lgl^{GX} (lgl^{KO}) and crb^{GX} (crb^{KO}) and knock-in alleles of *lgl::GFP* and lgl^{S5A}*::GFP* were previously described (Dong et al., 2015; Huang et al., 2009). *w; UAS-Crb*; (gift from Dr. Eli Knust, Dresden, Germany), *w par-6*$^{\Delta 226}$ *FRT*$^{9\text{-}2}$*/FM6* (gift from Dr. Jurgern Knoblich, Research Institute of Molecular Pathology, Vienna, Austria), *y w; DaPKC*^{k06403}*/CyO* (BL#10622), *w; His2Av::mRFP* (BL#23651), *y w ubi-GFP*^{NLS} *FRT*$^{9\text{-}2}$ (BL#5154), *w; Act5C(FRT.CD2)-Gal4, UAS-RFP/TM3, Sb* (BL#30558), *w; FRT*^{G13} *DaPKC*^{k06403}*/CyO; ubi-DaPKC::GFP/TM6, w; FRT*^{G13} *DaPKC*^{k06403}*/CyO; ubi-DaPKC*^{KR8Q}*::GFP/TM6, w par-6::GFP hs-FLP par-6*$^{\Delta 226}$ *FRT*$^{9\text{-}2}$*/FM7C, w; lgl::GFP hs-FLP*^{38}*; Act5C(FRT.CD2)-Gal4, UAS-RFP/TM3, Sb, w; lgl::GFP UAS-Crb/CyO, w; lgl*^{S5A}*::GFP UAS-Crb/CyO, w; lgl*^{S5A}*::GFP/CyO; hs-FLP Act5C(FRT.CD2)-Gal4, UAS-RFP/TM3, w hs-FLP; FRT*^{G13} *His2Av::mRFP, w par-6::GFP hs-FLP par-6*$^{\Delta 226}$ *FRT*$^{9\text{-}2}$*/FM7C; lgl*^{GX} *FRT*^{40A}*/CyO, w par-6::GFP hs-FLP par-6*$^{\Delta 226}$ *FRT*$^{9\text{-}2}$*/FM7C; ubi-RFP*^{NLS} *FRT*^{40A}*/CyO, w; lgl::GFP UAS-aPKC-CAAX* (*UAS-aPKC-CAAX*, gift from Dr. Sonsoles Campuzano, Univerisidad Autonoma de Madrid, Spain), *w UASp>mRFP::FKBP-5Ptase* (FKBP-INPP5E) and *w; UASp>Lck-FRB::CFP*, gifts from Dr. De Renzis, European Molecular Biology Laboratory, Heidelberg, Germany (Reversi et al., 2014), *w; αTub67C-Gal4*^{V2H}*; αTub67C-Gal4*^{V37} (Mat-Gal4, gift from Dr. Mark Peifer, University of North Carolina at Chapel Hill, NC; Schaefer et al., 2018), *w; GFP::aPKC/CyO* (gift from Dr. Daniel St Johnston, The Gurdon Institute, Cambridge, UK), and *w; UAS-Cdc42*^{CA} (BL#4854), *UAS-cdc42-RNAi, w;* (BL#29004), *y, v; UAS-DaPKC-RNAi* (BL#25946), *y, v; UAS-Par-6-RNAi* (BL#39010), *y, v; UAS-crb-RNAi* (BL#38373), *w; UAS-DaPKC-CAAX, w; UAS-DaPKC-CAAX, UAS-Par-6; w;; UAS-Par-6* (gifts from Dr. Tony Harris, University of Toronto, Toronto, Canada).

Transgenic flies of *ubi-DaPKC::GFP*, *ubi-aPKC*^{KR8Q}*::GFP*, and *par-6::GFP* were generated by phiC31-mediated integration protocol (Huang et al., 2009). *attP*^{VK00033} (BL#24871) stock was used to integrate ubi-DaPKC::GFP and ubi-DaPKC^{KR8Q}::GFP constructs into the third chromosome, and *attP*^{ZH2A} (BL#24480) stock was used to integrate par-6::GFP constructs into the X chromosome. *par-6::GFP* was further recombined with *par-6*$^{\Delta 226}$ null allele to generate *w par-6::GFP par-6*$^{\Delta 226}$, of which homozygote females and hemizygote males are fully viable and fertile, indicating a complete rescue of *par-6*$^{\Delta 226}$ by *par-6::GFP*. *Drosophila* cultures and genetic crosses were performed at 25°C. Detailed information about the strains from Bloomington Stock Center can be found in FlyBase.

Molecular cloning

To make ubi-aPKC::GFP, ubiquitin promoter (1,872 bp) was PCR-amplified from plasmid pWUM6 (gift from Dr. Jeff Sekelsky,

University of North Carolina at Chapel Hill, NC) using primers 5′-AGTGTCGAATTCCGCGCAGATCGCCGATGGGC-3′ and 5′-CTG GACGCGGCCGCGGTGGATTATTCTGCGGG-3′ and inserted into pGE-attB vector (Huang et al., 2009) to generate vector pGU. DNA fragments encoding aPKC::GFP and aPKC^{KR8Q}::GFP were then inserted into pGU vector. To make *par-6::GFP*, a 4.3-kb *par-6* genome DNA including 1-kbp upstream and 250-bp downstream sequences was PCR-amplified from *Drosophila* genomic DNA using primers 5′-ATGCGGCCGCGCTCTTCGGCTCTCGGA TAGTCG-3′ and 5′-GACGCGTGATTAAGGCCCGGCTAATG-3′, subcloned into pGE-attB vector. AvrII enzyme site was added before stop code for GFP insertion. More details about DNA constructs used in this study are in Table S1. NCBI: Par-6 (human), NP_058644.1; Lgl (mouse), NP_001152877.1. Plasmids containing PKCζ and PKCι coding sequences were gifts from Dr. Jane Wang (University of Pittsburgh, Pittsburgh, PA)

Live imaging and hypoxia treatment of aPKC::GFP and Par-6::GFP in *Drosophila* epithelial cells

Embryos and dissected ovaries were imaged according to a previously described protocol (Dong et al., 2015; Huang et al., 2011). Embryos were collected overnight at 25°C. Ovaries from adult females several days old were dissected in halocarbon oil (#95). Dechorinated embryos or dissected ovaries were mounted in halocarbon oil on an air-permeable membrane (YSI Membrane Model 5793; YSI) sealed by vacuum grease on a custom-made plastic slide over a 10 × 10–mm cut-through window. After placing the coverslip on top, a membrane at the bottom ensures sufficient air exchange to samples during the imaging session. The slide was then mounted in an air-tight microchamber (custom made) for live imaging under a confocal microscope. Oxygen levels inside the chamber were controlled by flow of either air or custom O_2/N_2 gas at the rate of ∼1–5 cc/s. Images were captured at room temperature (25°C) on a Leica TCS-NT confocal microscope (PL APO 40× oil objective, NA 1.25) by Leica TCS-NT software; an Olympus FV1000 confocal microscope (40× Uplan FL N oil objective, NA 1.3) by Olympus FV10-ASW software; or a Nikon A1 confocal microscope (Plan Fluo 40′ oil objective, NA 1.3) by NIS-Elements AR software. Images were further processed in ImageJ (National Institutes of Health) and Adobe Photoshop.

Purification of PKCζ and PKCζ/Par-6 complex from cultured cells

GST-PKCζ (gift from Dr. Ricardo Biondi, Instituto de Investigación en Biomedicina de Buenos Aires, Buenos Aires, Argentina; Zhang et al., 2014), GST-PKCζ^{KR8Q}, and Par-6::Hisx6 were expressed in Expi293F cells via transfection using the ExpiFectamine Transfection Kit (Gibco). Approximately 22.5 × 10^7 suspension-adapted Expi293F cells were diluted in Expi293 Expression Medium to a final volume of 76.5 ml and cultured in a 37°C shaker (Eppendorf New Brunswick S41i). 90 µg of plasmid DNA was mixed with 240 µl Expifectamine reagent into a total final volume of 9 ml Opti-MEM medium and incubated for 25 min. The mixture was then added to Expi293F cells to a total volume of 85.5 ml. After 18 h of incubation in the 37°C shaker, 450 µl of Transfection Enhancer I and 4.5 ml of Transfection Enhancer II were added to the cells. Cells were harvested after another 18 h of incubation, resuspended in 50 ml PBS buffer, and homogenized with an ice-cold tight-fitting Dounce homogenizer. To purify PKCζ/Par-6 or PKCζ^{KR8Q}/Par-6 complex, cells expressing Par-6::His6 were mixed with an equal volume of cells expressing GST-PKCζ or GST-PKCζ^{KR8Q} and homogenized. After centrifuging, supernatants from lysates were collected for purification by Pierce Glutathione Agarose. Bacteria BL21 was used to express and purify GST and GST fusion of aPKC PSr proteins as previously described (Dong et al., 2015).

Liposome pull-down assays

Liposomal binding assays were performed as described (Kim et al., 2008). To prepare liposomes, a lipid mixture of 37.5% phosphatidylcholine (840051C), 10% phosphatidylserine (840032C), 37.5% phosphatidylethanolamine (840021C), 10% cholesterol (700000P), and 5% PIP_2 (840046X) or PI4P (840045X, all lipids purchased from Avanti Polar Lipids) was dried and resuspended to a final concentration of 1 mg/ml of total phospholipids in Hepes buffer. After 30-min sonication, formed liposomes were harvested at 16,000 *g* for 10 min and resuspended in binding buffer (Hepes 20 mM, pH 7.4, KCl 120 mM, NaCl 20 mM, EGTA 1 mM, MgCl 1 mM, and BSA 1 mg/ml). In each liposome-binding assay, ∼0.1 µg of purified protein or protein complex was mixed with 50 µl of liposome suspension. After 15-min incubation at room temperature, liposomes were pelleted at 16,000 *g* for 10 min and were analyzed by Western blot to detect cosediments of target proteins.

Cell culture and imaging

HEK293 cells were cultured in glass-bottom dishes (In Vitro Scientific) and transfected with DNA using X-treme Gene 9 DNA transfection reagent (6365787001; Sigma-Aldrich). After 24–40 h of transfection, cells were mounted and imaged on an Olympus FV1000 confocal microscope (40× Uplan FL N oil objective, NA 1.3) by Olympus FV10-ASW software or a Nikon A1 confocal microscope (Plan Fluo 40× oil objective, NA 1.3) by NIS-Elements AR software. For images to be used for quantification, parameters were carefully adjusted to ensure no or minimum overexposure. In addition, when necessary, a fluorescent PM dye (CellMask DeepRed Plasma Membrane Stain, C10046; Thermo Fisher Scientific) was added to cell culture before live imaging to help visualize the PM for later quantifications. MDCK II cells were cultured in MEMα medium containing 10% FBS (Gibco) and 1% penicillin and streptomycin (Gibco). For growing polarized monolayers, MDCK cells were cultured on 0.4-µm Transwell filters (Corning) for 3 d. Transfection assays were performed on day 4 using Lipofectamine 2000 (Thermo Fisher Scientific), and cells were imaged on day 5.

Quantification of PM localization

PM localization were measured in ImageJ by custom macro scripts. For each image, PM masks were generated by an à trous wavelet decomposition method (Hammond et al., 2014; Olivo-Marin, 2002) based on the channel that contained either PM-localized proteins or fluorescent PM dyes. Cytosol masks were generated by segmentation using a threshold based on the mean

pixel value of the region of interest (ROI). Cells expressing all transfected fluorescent proteins were selected for measurement by drawing ROIs around each cell. Because of the use of computer-generated PM and cytosol masks, the exact shape of the ROI was not critical except that PM segments in contact with neighboring expressing cells were avoided. Custom macros were used to automatically measure PM and cytosolic intensities of each fluorescent protein in each cell marked by an ROI in the sample image. Backgrounds were autodetected by the macro based on the minimal pixel value of the whole image. The PM localization index for each fluorescent protein was calculated by the macro as the ratio of (PM – background)/(cytosol – background). Data were further processed in Excel and visualized and analyzed in GraphPad Prism.

Biochemistry

For Lgl-phosphorylation assay, HEK293 cells were cultured in DMEM supplemented with 10% FBS. 24 h after transient transfection, cells were directly lysed in SDS loading buffer, and equal volumes of cell lysates were resolved in 12% SDS-PAGE. Proteins were detected by Western blot using antibody chicken anti-GFP, 1:5,000 (GFP-1020; Aves Lab); rabbit anti-phospho-mLgl, 1:1,000 (AP2198a; Abgent); rabbit anti-PKC, 1:5,000 (pan-aPKC antibody, Santa Cruz, Sc-216); PKCζ-specific antibody (C24E6); rabbit mAb (Cell Signaling, 9368); or mouse anti-Flag 1:5,000 (F3165; Sigma-Aldrich). For immunoprecipitation experiments, cells were lysed in radioimmunoprecipitation assay buffer (25 mM Tris-HCl, pH 7.4, 150 mM NaCl, 0.1% SDS, 0.5% sodium deoxycholate, and 1% Triton X-100). Protein G-Sepharose beads were incubated with homemade, affinity-purified rabbit anti-GFP antibody (Huang et al., 2009) for 1 h followed by incubation with the equal amount of each lysate for 1 h. The beads were washed and boiled with SDS loading buffer. Supernatants were detected by Western blot.

Induction of FKBP12-phosphatase and Lyn11-FRB::CFP dimerization in HEK293 cells

The procedure has been described in detail previously (Hammond et al., 2014). In brief, HEK293 cells cultured in 35-mm glass-bottom dishes (In Vitro Scientific) were transiently transfected with 1 µg total DNA, which included the Lyn11-FRB::CFP recruiter, FKBP12 phosphatases (Hammond et al., 2012), PKCζ::GFP, and Par-6::iRFP as indicated. After 22–26 h, cells were imaged in Fluoro-Brite medium (Life Technologies) using a Nikon A1R confocal laser scanning microscope though a 100×, NA/1.45 plan apochromatic objective lens. Time-lapse imaging started 2 min before bath addition of 1 µM rapamycin. CFP::Lyn11-FRB images were used to generate binary masks to define PM. PM localization of each reporter was then calculated from the ratio of fluorescence within the PM to the whole cell and was expressed relative to the average before rapamycin addition (Hammond et al., 2014).

Induction of mRFP::FKBP-5Ptase and Lck-FRB::CFP dimerization in live *Drosophila* follicular cells

Young females of w UASp>mRFP::FKBP-5Ptase / w par-6::GFP par-6$^{\Delta 226}$; hs-FLP Act5C(FRT.CD2)-Gal4 UAS-RFP/UASp>Lck-FRB::CFP or w UASp>mRFP::FKBP-5Ptase / +; lgl::GFP hs-FLP /+; Act5C(FRT.CD2)-Gal4 UAS-RFP / UASp>Lck-FRB::CFP were heat-shocked at 37°C for 1 h. Ovaries were dissected 4 d later in 1× PBS, mounted in a drop of 20 µl Schneider's medium containing 10 µM rapamycin on a gas-permeable slide, and imaged live, as previously described (Huang et al., 2011; Dong et al., 2015). Treated lgl::GFP ovaries served as a positive control (Dong et al., 2015).

Generation of mitotic mutant clones in *Drosophila* follicular epithelia

Mutant follicular cell clones of lgl^{KO} or $aPKC^{k06403}$ were generated by the routine FLP/FRT technique. Young females were heat-shocked at 37°C for 1 h, and their ovaries were dissected 3 d later.

Immunostaining and confocal imaging

Immunostaining of embryos and adult ovaries was performed as described (Huang et al., 2009). Primary antibodies: rabbit anti-GFP (Huang et al., 2009) 1:1,500; chicken anti-GFP (Aves Lab) 1:1,000; rabbit anti-Lgl (d-300, Santa Cruz) 1:200; and rabbit anti-aPKC (Santa Cruz) 1:1,000. Secondary antibodies: Cy2-, Cy3-, or Cy5-conjugated goat anti-rabbit IgG, anti-chicken IgG, goat anti-rat IgG, goat anti-mouse IgG, and goat anti-guinea pig IgG (Jackson ImmunoResearch Lab), all at 1:400. Images were collected on an Olympus FV1000 confocal microscope and processed in Adobe Photoshop and ImageJ.

Genotypes of *Drosophila* samples in figures

Fig. 1 C: w; FRT^{G13} DaPKC^{k06403} / CyO; ubi-DaPKC::GFP / TM6; w; FRT^{G13} DaPKC^{k06403} / CyO; ubi-DaPKC^{KR8Q}::GFP / TM6. Fig. 1 D: w; FRT^{G13} DaPKC^{k06403} / CyO; ubi-DaPKC::GFP / TM6; w par-6::GFP hs-FLP par-6$^{\Delta 226}$ FRT$^{9-2}$. Fig. 3 B: Top: w; GFP::aPKC / UAS-Cdc42^{CA}; hs-FLP Act5C(FRT.CD2)-Gal4 UAS-RFP / +. Bottom: w; UAS-Cdc42^{CA} / +; hs-FLP Act5C(FRT.CD2)-Gal4 UAS-RFP / ubi-DaPKC^{KR8Q}::GFP. Fig. 3 C: UAS-cdc42-RNAi, w / w; GFP::aPKC / +; hs-FLP Act5C(FRT.CD2)-Gal4 UAS-RFP / +. Fig. 8, A and B: w; lgl::GFP hs-FLP/ lgl::GFP UAS-crb; Act5C(FRT.CD2)-Gal4 UAS-RFP / +; w; lgl^{S5A}::GFP UAS-Crb / +; hs-FLP Act5C(FRT.CD2)-Gal4 UAS-RFP / +. Fig. 8 C: w; lgl::GFP UAS-Crb / +; +/+; w; lgl::GFP UAS-Crb / αTub67C-Gal4^{V2H}; αTub67C-Gal4^{V37}/ +; w; lgl^{S5A}::GFP UAS-Crb / αTub67C-Gal4^{V2H}; αTub67C-Gal4^{V37}/ +. Fig. 8 D: w; lgl::GFP; w; lgl::GFP; crb^{KO}/ crb^{KO}. Fig. 8 E: w; lgl::GFP UAS-Crb / +; hs-FLP Act5C(FRT.CD2)-Gal4 UAS-RFP / UAS-DaPKC-RNAi. Fig. 8 F: w; lgl::GFP UAS-Crb / UAS-par6-RNAi; hs-FLP Act5C(FRT.CD2)-Gal4 UAS-RFP / +. Fig. 8 G: w; lgl::GFP hs-FLP / +; Act5C(FRT.CD2)-Gal4 UAS-RFP / UAS-DaPKCΔN. Fig. S1 A: w / w hs-FLP; FRT^{G13} DaPKC^{k06403}/ FRT^{G13} His2Av::mRFP; ubi-DaPKC::GFP/+; w / w hs-FLP; FRT^{G13} DaPKC^{k06403}/ FRT^{G13} His2Av::mRFP; ubi-DaPKC^{KR8Q}::GFP/+. Fig. S1 B: w par-6::GFP hs-FLP par-6$^{\Delta 226}$ FRT$^{9-2}$/FM7C; w; FRT^{G13} DaPKC^{k06403}/CyO; ubi-aPKC::GFP/TM6. Fig. S1 C: w par-6::GFP hs-FLP par-6$^{\Delta 226}$ FRT$^{9-2}$/ w; lgl^{KO} FRT^{40A}/ ubi-RFP^{NLS} FRT^{40A}. Fig. S3, A and B: w UAS-mRFP-FKBP-5′Ptas / par-6::GFP hs-FLP par-6$^{\Delta 226}$ FRT$^{9-2}$; +/+; Act5C(FRT.CD2)- UAS-RFP^{NLS}/ UAS-lck-FRB::CFP.

Online supplemental material

Fig. S1 shows that the polybasic PSr was required for PM targeting of *Drosophila* aPKC, and both Par-6::GFP and DaPKC::GFP

showed hypoxia-sensitive PM localization in embryonic epithelia. In addition, hypoxia-sensitive PM localization of Par-6::GFP was not affected by the loss of Lgl. Fig. S2 shows that in MCF7, COS7, and polarized MDCK cells, PM targeting of PKCζ required coexpression of Par-6. Fig. S3 shows that acute depletion of PIP_2 in *Drosophila* follicular cells did not strongly inhibit the PM localization of Par-6::GFP. Fig. S4 shows that Crb-intra was capable of recruiting Par-6 to PM in HEK293 cells, and that Lgl::GFP PM localization in polarized MDCK cells is resistant to the overexpression of PKCζ::RFP. Videos 1 and 2 show the acute and reversible loss of DaPKC::GFP and Par-6::GFP from PM under hypoxia in live *Drosophila* follicular cells. Table S1 lists the details about DNA constructs.

Acknowledgments

We are grateful to Drs. Jane Wang, Gerald Apodoca, Mark Peifer, Eli Knust, Thomas Weide, David Bilder, Tony Harris, Daniel St Johnston, Jean Wilson, and Ricardo Biondi for reagents and fly stocks; Lu Jiang and Kriti Sanghi for technical assistance; Dr. Marijn Ford for help on protein purification; Dr. Simon Watkins and University of Pittsburgh Medical School Center for Biological Imaging for generous imaging and microscopy support; Bloomington Stock Center for fly stocks; and Developmental Studies Hybridoma Bank for antibodies.

This work was supported by National Institutes of Health, National Center for Research Resources (R21RR024869 to Y. Hong), National Institutes of Health, National Institute of General Medical Sciences (R01GM086423 and R01GM121534 to Y. Hong), and National Institutes of Health (1R35GM119412-01 to G.R. Hammond). The University of Pittsburgh Medical School Center for Biological Imaging is supported by National Institutes of Health grant 1S10OD019973-01.

The authors declare no competing financial interests.

Author contributions: Conceptualization: Y. Hong, W. Dong, G.R. Hammond; Investigation: W. Dong, J. Lu, X. Zhang, Y. Wu, K. Lettieri, G.R. Hammond, Y. Hong; Writing–Review & Editing: Y. Hong, W. Dong, G.R. Hammond; Funding acquisition: Y. Hong, G.R. Hammond; Supervision: Y. Hong.

Submitted: 19 March 2019
Revised: 4 March 2020
Accepted: 19 April 2020

References

Arbuzova, A., A.A. Schmitz, and G. Vergères. 2002. Cross-talk unfolded: MARCKS proteins. *Biochem. J.* 362:1–12. https://doi.org/10.1042/bj3620001

Atwood, S.X., C. Chabu, R.R. Penkert, C.Q. Doe, and K.E. Prehoda. 2007. Cdc42 acts downstream of Bazooka to regulate neuroblast polarity through Par-6 aPKC. *J. Cell Sci.* 120:3200–3206. https://doi.org/10.1242/jcs.014902

Bailey, M.J., and K.E. Prehoda. 2015. Establishment of Par-Polarized Cortical Domains via Phosphoregulated Membrane Motifs. *Dev. Cell.* 35:199–210. https://doi.org/10.1016/j.devcel.2015.09.016

Betschinger, J., K. Mechtler, and J.A. Knoblich. 2003. The Par complex directs asymmetric cell division by phosphorylating the cytoskeletal protein Lgl. *Nature.* 422:326–330. https://doi.org/10.1038/nature01486

Brzeska, H., J. Guag, K. Remmert, S. Chacko, and E.D. Korn. 2010. An experimentally based computer search identifies unstructured membrane-binding sites in proteins: application to class I myosins, PAKS, and CARMIL. *J. Biol. Chem.* 285:5738–5747. https://doi.org/10.1074/jbc.M109.066910

Chabu, C., and C.Q. Doe. 2008. Dap160/intersectin binds and activates aPKC to regulate cell polarity and cell cycle progression. *Development.* 135:2739–2746. https://doi.org/10.1242/dev.024059

Chan, H.Y., S. v, X. Xing, P. Kraus, S.P. Yap, P. Ng, S.L. Lim, and T. Lufkin. 2011. Comparison of IRES and F2A-based locus-specific multicistronic expression in stable mouse lines. *PLoS One.* 6. e28885. https://doi.org/10.1371/journal.pone.0028885

Chen, J., A.-C. Sayadian, N. Lowe, H.E. Lovegrove, and D. St Johnston. 2018. An alternative mode of epithelial polarity in the Drosophila midgut. *PLoS Biol.* 16. e3000041. https://doi.org/10.1371/journal.pbio.3000041

Dickinson, D.J., F. Schwager, L. Pintard, M. Gotta, and B. Goldstein. 2017. A Single-Cell Biochemistry Approach Reveals PAR Complex Dynamics during Cell Polarization. *Dev. Cell.* 42:416–434.e11. https://doi.org/10.1016/j.devcel.2017.07.024

Dong, W., X. Zhang, W. Liu, Y.J. Chen, J. Huang, E. Austin, A.M. Celotto, W.Z. Jiang, M.J. Palladino, Y. Jiang, et al. 2015. A conserved polybasic domain mediates plasma membrane targeting of Lgl and its regulation by hypoxia. *J. Cell Biol.* 211:273–286. https://doi.org/10.1083/jcb.201503067

Fletcher, G.C., E.P. Lucas, R. Brain, A. Tournier, and B.J. Thompson. 2012. Positive feedback and mutual antagonism combine to polarize Crumbs in the Drosophila follicle cell epithelium. *Curr. Biol.* 22:1116–1122. https://doi.org/10.1016/j.cub.2012.04.020

Garg, R., L.G. Benedetti, M.B. Abera, H. Wang, M. Abba, and M.G. Kazanietz. 2014. Protein kinase C and cancer: what we know and what we do not. *Oncogene.* 33:5225–5237.

Georgiou, M., E. Marinari, J. Burden, and B. Baum. 2008. Cdc42, Par6, and aPKC regulate Arp2/3-mediated endocytosis to control local adherens junction stability. *Curr. Biol.* 18:1631–1638. https://doi.org/10.1016/j.cub.2008.09.029

Graybill, C., B. Wee, S.X. Atwood, and K.E. Prehoda. 2012. Partitioning-defective protein 6 (Par-6) activates atypical protein kinase C (aPKC) by pseudosubstrate displacement. *J. Biol. Chem.* 287:21003–21011. https://doi.org/10.1074/jbc.M112.360495

Hammond, G.R., M.P. Machner, and T. Balla. 2014. A novel probe for phosphatidylinositol 4-phosphate reveals multiple pools beyond the Golgi. *J. Cell Biol.* 205:113–126. https://doi.org/10.1083/jcb.201312072

Hammond, G.R.V.. 2012. Membrane biology: Making light work of lipids. *Curr. Biol.* 22:R869–R871. https://doi.org/10.1016/j.cub.2012.09.005

Hammond, G.R.V., M.J. Fischer, K.E. Anderson, J. Holdich, A. Koteci, T. Balla, and R.F. Irvine. 2012. PI4P and PI(4,5)P2 are essential but independent lipid determinants of membrane identity. *Science.* 337:727–730. https://doi.org/10.1126/science.1222483

Hammond, G.R.V., Y. Sim, L. Lagnado, and R.F. Irvine. 2009. Reversible binding and rapid diffusion of proteins in complex with inositol lipids serves to coordinate free movement with spatial information. *J. Cell Biol.* 184:297–308. https://doi.org/10.1083/jcb.200809073

Heo, W.D., T. Inoue, W.S. Park, M.L. Kim, B.O. Park, T.J. Wandless, and T. Meyer. 2006. PI(3,4,5)P3 and PI(4,5)P2 lipids target proteins with polybasic clusters to the plasma membrane. *Science.* 314:1458–1461. https://doi.org/10.1126/science.1134389

Hong, Y.. 2018. aPKC: the Kinase that Phosphorylates Cell Polarity. *F1000 Res.* 7:903. https://doi.org/10.12688/f1000research.14427.1

Hong, Y., L. Ackerman, L.Y. Jan, and Y.N. Jan. 2003. Distinct roles of Bazooka and Stardust in the specification of Drosophila photoreceptor membrane architecture. *Proc. Natl. Acad. Sci. USA.* 100:12712–12717. https://doi.org/10.1073/pnas.2135347100

Huang, J., L. Huang, Y.-J. Chen, E. Austin, C.E. Devor, F. Roegiers, and Y. Hong. 2011. Differential regulation of adherens junction dynamics during apical-basal polarization. *J. Cell Sci.* 124:4001–4013. https://doi.org/10.1242/jcs.086694

Huang, J., W. Zhou, W. Dong, A.M. Watson, and Y. Hong. 2009. From the Cover: Directed, efficient, and versatile modifications of the Drosophila genome by genomic engineering. *Proc. Natl. Acad. Sci. USA.* 106:8284–8289. https://doi.org/10.1073/pnas.0900641106

Hurd, T.W., L. Gao, M.H. Roh, I.G. Macara, and B. Margolis. 2003. Direct interaction of two polarity complexes implicated in epithelial tight junction assembly. *Nat. Cell Biol.* 5:137–142. https://doi.org/10.1038/ncb923

Hutterer, A., J. Betschinger, M. Petronczki, and J.A. Knoblich. 2004. Sequential roles of Cdc42, Par-6, aPKC, and Lgl in the establishment of

epithelial polarity during Drosophila embryogenesis. *Dev. Cell*. 6:845–854. https://doi.org/10.1016/j.devcel.2004.05.003

Izumi, Y., T. Hirose, Y. Tamai, S. Hirai, Y. Nagashima, T. Fujimoto, Y. Tabuse, K.J. Kemphues, and S. Ohno. 1998. An atypical PKC directly associates and colocalizes at the epithelial tight junction with ASIP, a mammalian homologue of Caenorhabditis elegans polarity protein PAR-3. *J. Cell Biol*. 143:95–106. https://doi.org/10.1083/jcb.143.1.95

Joberty, G., C. Petersen, L. Gao, and I.G. Macara. 2000. The cell-polarity protein Par6 links Par3 and atypical protein kinase C to Cdc42. *Nat. Cell Biol*. 2:531–539. https://doi.org/10.1038/35019573

Kempkens, O., E. Médina, G. Fernandez-Ballester, S. Ozüyaman, A. Le Bivic, L. Serrano, and E. Knust. 2006. Computer modelling in combination with in vitro studies reveals similar binding affinities of Drosophila Crumbs for the PDZ domains of Stardust and DmPar-6. *Eur. J. Cell Biol*. 85:753–767. https://doi.org/10.1016/j.ejcb.2006.03.003

Kim, A.Y., Z. Tang, Q. Liu, K.N. Patel, D. Maag, Y. Geng, and X. Dong. 2008. Pirt, a phosphoinositide-binding protein, functions as a regulatory subunit of TRPV1. *Cell*. 133:475–485. https://doi.org/10.1016/j.cell.2008.02.053

Kim, M., A. Datta, P. Brakeman, W. Yu, and K.E. Mostov. 2007. Polarity proteins PAR6 and aPKC regulate cell death through GSK-3β in 3D epithelial morphogenesis. *J. Cell Sci*. 120:2309–2317. https://doi.org/10.1242/jcs.007443

Kim, S., I. Gailite, B. Moussian, S. Luschnig, M. Goette, K. Fricke, M. Honemann-Capito, H. Grubmüller, and A. Wodarz. 2009. Kinase-activity-independent functions of atypical protein kinase C in Drosophila. *J. Cell Sci*. 122:3759–3771. https://doi.org/10.1242/jcs.052514

Krahn, M.P., J. Bückers, L. Kastrup, and A. Wodarz. 2010. Formation of a Bazooka-Stardust complex is essential for plasma membrane polarity in epithelia. *J. Cell Biol*. 190:751–760. https://doi.org/10.1083/jcb.201006029

Lin, D., A.S. Edwards, J.P. Fawcett, G. Mbamalu, J.D. Scott, and T. Pawson. 2000. A mammalian PAR-3-PAR-6 complex implicated in Cdc42/Rac1 and aPKC signalling and cell polarity. *Nat. Cell Biol*. 2:540–547. https://doi.org/10.1038/35019582

McLaughlin, S., and D. Murray. 2005. Plasma membrane phosphoinositide organization by protein electrostatics. *Nature*. 438:605–611. https://doi.org/10.1038/nature04398

Morais-de-Sá, E., V. Mirouse, and D. St Johnston. 2010. aPKC phosphorylation of Bazooka defines the apical/lateral border in Drosophila epithelial cells. *Cell*. 141:509–523. https://doi.org/10.1016/j.cell.2010.02.040

Olivo-Marin, J.-C.. 2002. Extraction of spots in biological images using multiscale products. *Pattern Recognit*. 35:1989–1996. https://doi.org/10.1016/S0031-3203(01)00127-3

Pellikka, M., G. Tanentzapf, M. Pinto, C. Smith, C.J. McGlade, D.F. Ready, and U. Tepass. 2002. Crumbs, the Drosophila homologue of human CRB1/RP12, is essential for photoreceptor morphogenesis. *Nature*. 416:143–149. https://doi.org/10.1038/nature721

Qiu, R.G., A. Abo, and G. Steven Martin. 2000. A human homolog of the C. elegans polarity determinant Par-6 links Rac and Cdc42 to PKCzeta signaling and cell transformation. *Curr. Biol*. 10:697–707. https://doi.org/10.1016/S0960-9822(00)00535-2

Reversi, A., E. Loeser, D. Subramanian, C. Schultz, and S. De Renzis. 2014. Plasma membrane phosphoinositide balance regulates cell shape during Drosophila embryo morphogenesis. *J. Cell Biol*. 205:395–408. https://doi.org/10.1083/jcb.201309079

Rodriguez, J., F. Peglion, J. Martin, L. Hubatsch, J. Reich, N. Hirani, A.G. Gubieda, J. Roffey, A.R. Fernandes, D. St Johnston, et al. 2017. aPKC Cycles between Functionally Distinct PAR Protein Assemblies to Drive Cell Polarity. *Dev. Cell*. 42:400–415.e9. https://doi.org/10.1016/j.devcel.2017.07.007

Rodriguez-Boulan, E., and I.G. Macara. 2014. Organization and execution of the epithelial polarity programme. *Nat. Rev. Mol. Cell Biol*. 15:225–242. https://doi.org/10.1038/nrm3775

Rosse, C., M. Linch, S. Kermorgant, A.J.M. Cameron, K. Boeckeler, and P.J. Parker. 2010. PKC and the control of localized signal dynamics. *Nat. Rev. Mol. Cell Biol*. 11:103–112. https://doi.org/10.1038/nrm2847

Schaefer, K.N., T.T. Bonello, S. Zhang, C.E. Williams, D.M. Roberts, D.J. McKay, and M. Peifer. 2018. Supramolecular assembly of the beta-catenin destruction complex and the effect of Wnt signaling on its localization, molecular size, and activity in vivo. *PLoS Genet*. 14. e1007339. https://doi.org/10.1371/journal.pgen.1007339

Sherrard, K.M., and R.G. Fehon. 2015. The transmembrane protein Crumbs displays complex dynamics during follicular morphogenesis and is regulated competitively by Moesin and aPKC. *Development*. 142:1869–1878. https://doi.org/10.1242/dev.115329

Sotillos, S., M.T. Díaz-Meco, E. Caminero, J. Moscat, and S. Campuzano. 2004. DaPKC-dependent phosphorylation of Crumbs is required for epithelial cell polarity in Drosophila. *J. Cell Biol*. 166:549–557. https://doi.org/10.1083/jcb.200311031

Stross, C., V. Keitel, E. Winands, D. Häussinger, and R. Kubitz. 2009. Expression and localization of atypical PKC isoforms in liver parenchymal cells. *Biol. Chem*. 390:235–244. https://doi.org/10.1515/BC.2009.031

Suzuki, A., and S. Ohno. 2006. The PAR-aPKC system: lessons in polarity. *J. Cell Sci*. 119:979–987. https://doi.org/10.1242/jcs.02898

Visco, I., C. Hoege, A.A. Hyman, and P. Schwille. 2016. In vitro Reconstitution of a Membrane Switch Mechanism for the Polarity Protein LGL. *J. Mol. Biol*. 428(24, 24 Pt A):4828–4842. https://doi.org/10.1016/j.jmb.2016.10.003

Walther, R.F., and F. Pichaud. 2010. Crumbs/DaPKC-dependent apical exclusion of Bazooka promotes photoreceptor polarity remodeling. *Curr. Biol*. 20:1065–1074. https://doi.org/10.1016/j.cub.2010.04.049

Wang, Q., T.W. Hurd, and B. Margolis. 2004. Tight junction protein Par6 interacts with an evolutionarily conserved region in the amino terminus of PALS1/stardust. *J. Biol. Chem*. 279:30715–30721. https://doi.org/10.1074/jbc.M401930200

Yamanaka, T., Y. Horikoshi, A. Suzuki, Y. Sugiyama, K. Kitamura, R. Maniwa, Y. Nagai, A. Yamashita, T. Hirose, H. Ishikawa, et al. 2001. PAR-6 regulates aPKC activity in a novel way and mediates cell-cell contact-induced formation of the epithelial junctional complex. *Genes Cells*. 6:721–731. https://doi.org/10.1046/j.1365-2443.2001.00453.x

Yeung, T., G.E. Gilbert, J. Shi, J. Silvius, A. Kapus, and S. Grinstein. 2008. Membrane phosphatidylserine regulates surface charge and protein localization. *Science*. 319:210–213. https://doi.org/10.1126/science.1152066

Yeung, T., M. Terebiznik, L. Yu, J. Silvius, W.M. Abidi, M. Philips, T. Levine, A. Kapus, and S. Grinstein. 2006. Receptor activation alters inner surface potential during phagocytosis. *Science*. 313:347–351. https://doi.org/10.1126/science.1129551

Zhang, H., S. Neimanis, L.A. Lopez-Garcia, J.M. Arencibia, S. Amon, A. Stroba, S. Zeuzem, E. Proschak, H. Stark, A.F. Bauer, et al. 2014. Molecular mechanism of regulation of the atypical protein kinase C by N-terminal domains and an allosteric small compound. *Chem. Biol*. 21:754–765. https://doi.org/10.1016/j.chembiol.2014.04.007

Zilberman, Y., J. Abrams, D.C. Anderson, and J. Nance. 2017. Cdc42 regulates junctional actin but not cell polarization in the *Caenorhabditis elegans* epidermis. *J. Cell Biol*. 216:3729–3744. https://doi.org/10.1083/jcb.201611061

Supplemental material

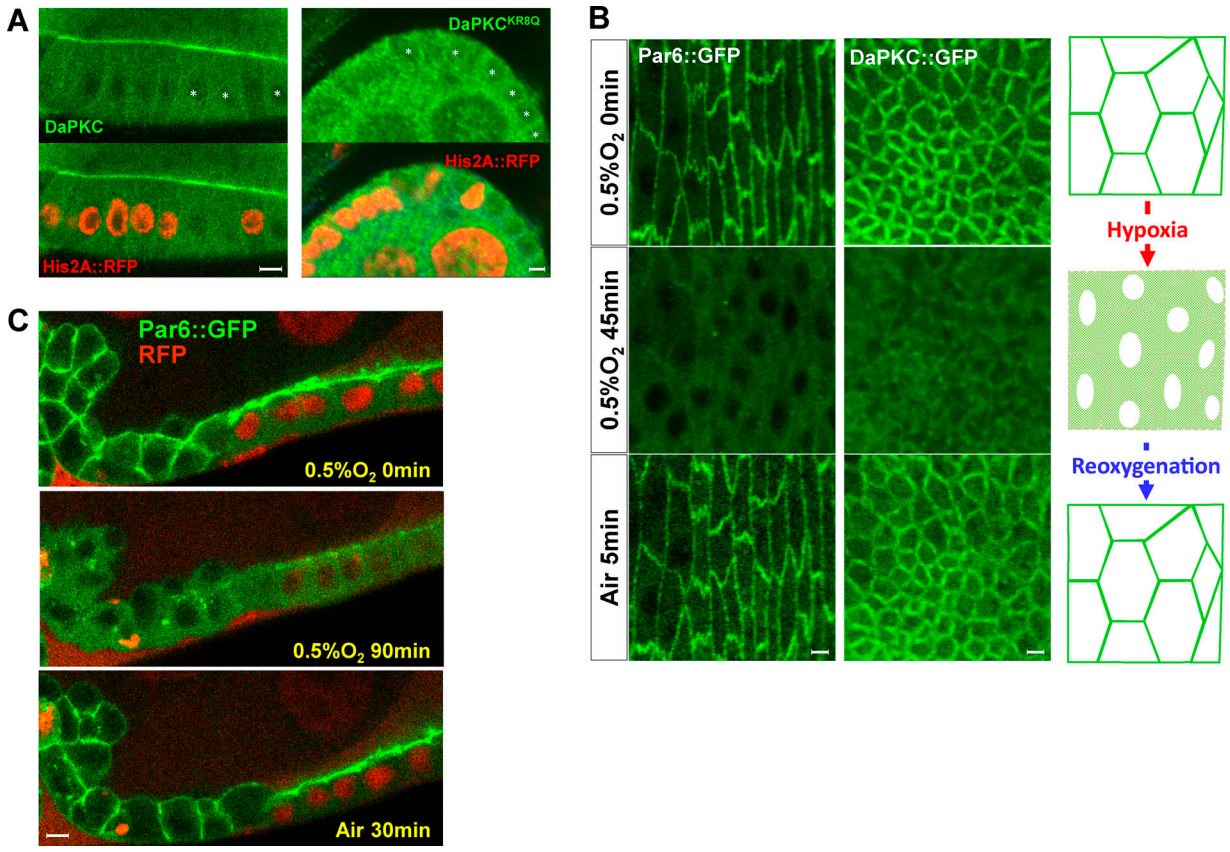

Figure S1. **Polybasic PSr is required for PM targeting of *Drosophila* aPKC. (A)** PM localization of wild-type DaPKC::GFP and nonpolybasic DaPKC^{KR8Q}::GFP in *Drosophila* wild type and *DaPKC*$^{-/-}$ mutant follicular epithelial cells. Asterisks indicate *DaPKC*$^{-/-}$ mutant cells identified by the loss of Histon2A::RFP (His2A::RFP). Images are in cross-section view. **(B)** In *Drosophila* embryonic epithelial cells, PM localization of Par-6::GFP or DaPKC::GFP was lost under hypoxia (0.5% O_2) but recovered after posthypoxia reoxygenation. Images are in tangential view of the apical surface of embryonic epithelia. **(C)** Par-6::GFP showed acute and reversible loss of PM targeting under hypoxia in both wild-type and *lgl*$^{-/-}$ mutant (marked by the loss of nuclear RFP) follicular epithelial cells. Note that in *lgl*$^{-/-}$ mutant cells, Par-6 was no longer restricted to apical PM but localized to both apical and lateral PM. Images are in cross-section view. Scale bars: 5 µm.

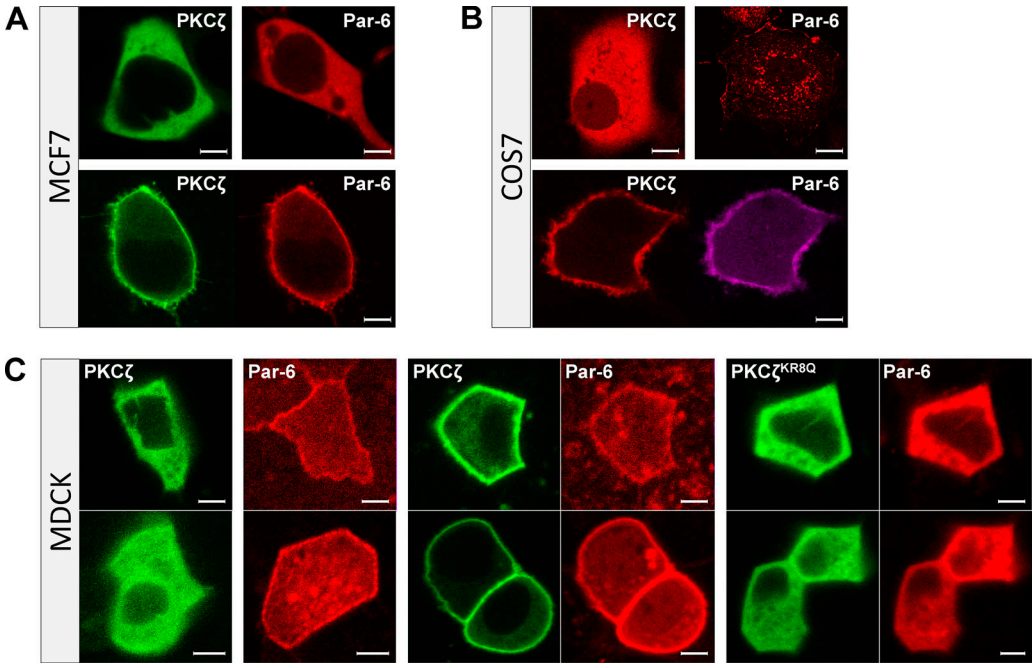

Figure S2. **Par-6–dependent PM targeting of PKCζ in MCF7, COS7, and polarized MDCK cells. (A and B)** Representative images showing that in MCF7 and COS7 cells, PKCζ and Par-6 were cytosolic when expressed alone, but both became PM-localized when coexpressed. **(C)** Representative images showing that in polarized MDCK cells, overexpressed PKCζ::GFP was cytosolic and Par-6::RFP was partially PM-localized. Both PKCζ::GFP and Par-6::RFP were PM-localized when coexpressed, whereas both PKCζ^{KR8Q}::GFP and Par-6::RFP were cytosolic when coexpressed. Scale bars: 5 µm.

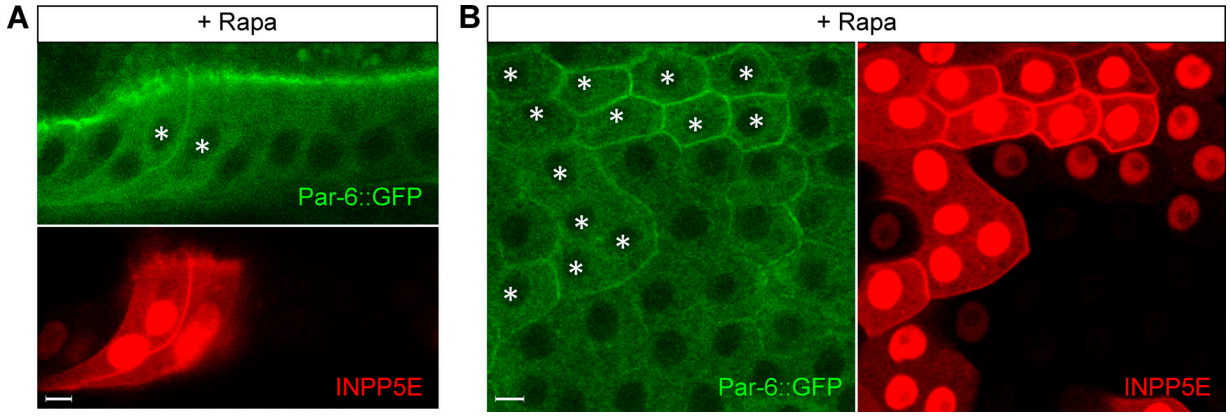

Figure S3. **Par-6::GFP expands to basolateral PM in *Drosophila* follicular epithelial cells under the acute loss of PIP_2.** Cells overexpressing mRFP-FKBP-INPP5E and PM-bound Lck-FRB::CFP (not depicted) are labeled by nuclear RFP (asterisks in GFP images). Rapamycin (rapa) treatment induced strong PM localization of mRFP-FKBP-INPP5E, but Par-6::GFP remained largely on apical PM (A, cross-section view) with expansion to lateral PM (B, tangential view of basolateral PM). Scale bars: 5 µm.

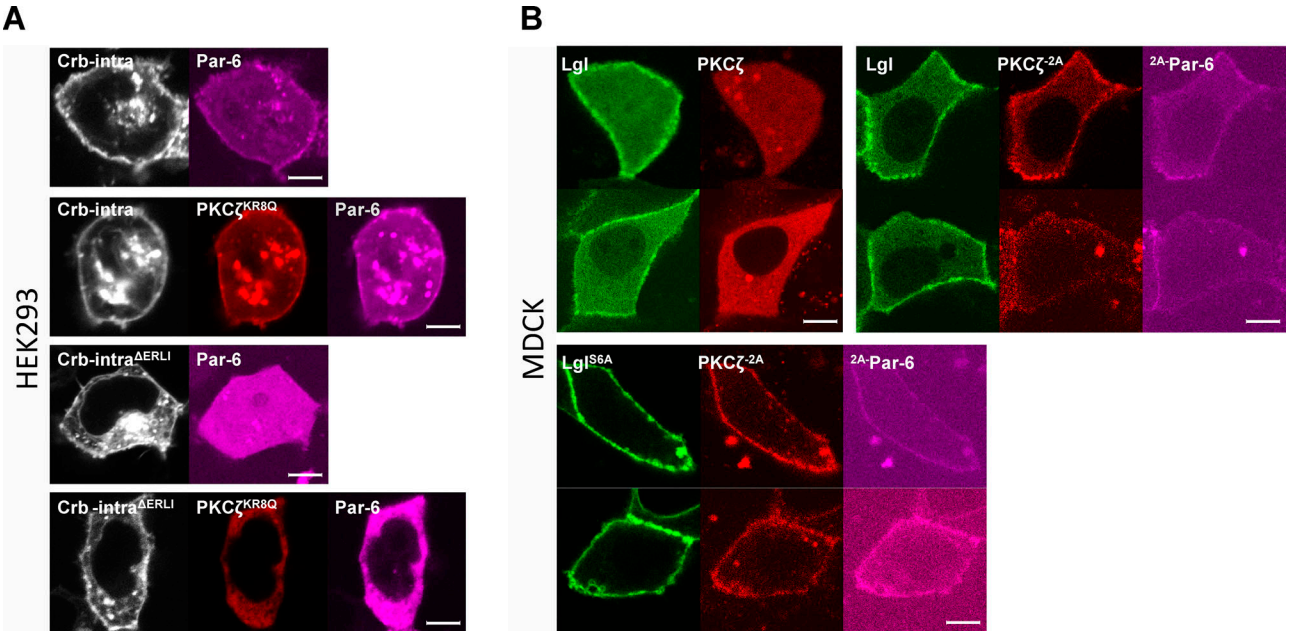

Figure S4. **Interaction between Par-6 and Crb-intra in HEK293 cells. (A)** Par-6::iRFP localized to PM in HEK293 cells expressing BFP::Crb-intra, but not in cells expressing BFP::Crb-intra$^{\Delta ERLI}$. PKCζ^{KR8Q}::RFP was PM-localized in cells expressing Par-6::iRFP and BFP::Crb-intra but was cytosolic in cells expressing Par-6::iRFP and BFP::Crb-intra$^{\Delta ERLI}$. **(B)** Lgl::GFP was predominantly PM-localized in polarized MDCK cells overexpressing PKCζ::RFP or PKCζ::RFP^{-2A}-Par-6::iRFP. Lgl^{S6A}::GFP was PM-localized in MDCK cells expressing PKCζ::RFP^{-2A}-Par-6::iRFP. Scale bars: 5 µm.

Video 1. **Acute and reversible loss of PM DaPKC::GFP under hypoxia.** Ovaries from a 3-d-old *ubi-DaPKC::GFP* female were dissected and imaged live in an environment-controlled microchamber. Hypoxic (0.5% O_2) gas was flashed into the chamber starting at 0 min. Normal air was flashed into the chamber starting at 42 min for reoxygenation. Time intervals are 3 min during hypoxia and 10 s during reoxygenation. Frame rate is 7 frames per second.

Video 2. **Acute and reversible loss of PM Par-6::GFP under hypoxia.** Ovaries from a 3-d-old genomically rescued *par-6::GFP par-6$^{\Delta 226}$* female were dissected and imaged live similarly as samples in Video 1. Reoxygenation starts from 33 min. Time intervals are 3 min during hypoxia and 10 s during reoxygenation. Frame rate is 7 frames per second.

Provided online is one table. Table S1 lists details about DNA constructs used in this study.